Journal of
Mechanics of
Materials and Structures

COUPLED THERMALLY GENERAL IMPERFECT AND MECHANICALLY COHERENT ENERGETIC INTERFACES SUBJECT TO IN-PLANE DEGRADATION

Ali Esmaeili, Paul Steinmann and Ali Javili

Volume 12, No. 3 May 2017

msp

JOURNAL OF MECHANICS OF MATERIALS AND STRUCTURES
Vol. 12, No. 3, 2017
dx.doi.org/10.2140/jomms.2017.12.289

COUPLED THERMALLY GENERAL IMPERFECT AND MECHANICALLY COHERENT ENERGETIC INTERFACES SUBJECT TO IN-PLANE DEGRADATION

ALI ESMAEILI, PAUL STEINMANN AND ALI JAVILI

To date, the effects of interface in-plane damage on the thermomechanical response of a thermally general imperfect (GI) and mechanically coherent energetic interface are not taken into account. A thermally GI interface allows for a discontinuity in temperature as well as in the normal heat flux across the interface. A mechanically coherent energetic interface permits a discontinuity in the normal traction but not in the displacement field across the interface. The temperature of a thermally GI interface is a degree of freedom and is computed using a material parameter known as the sensitivity. The current work is the continuation of the model developed by Esmaeili et al. (2016a) where a degrading highly conductive (HC) and mechanically coherent energetic interface is considered. An HC interface only allows for the jump in normal heat flux and not the jump in temperature across the interface. In this contribution, a thermodynamically consistent theory for thermally GI and mechanically coherent energetic interfaces subject to in-plane degradation is developed. A computational framework to model this class of interfaces using the finite element method is established. In particular, the influence of the interface in-plane degradation on the sensitivity is captured. To this end, the equations governing a fully nonlinear transient problem are given. They are solved using the finite element method. The results are illustrated through a series of three-dimensional numerical examples for various interfacial parameters. In particular, a comparison is made between the results of the intact and the degraded thermally GI interface formulation.

A list of symbols can be found on page 310.

1. Introduction

Interfaces possess different thermomechanical properties from those of the bulk. The interface properties become dominating as the length scale reduces: the smaller the scale, the larger the interface area to bulk volume ratio [Cammarata 1994; Dingreville et al. 2005; Duan et al. 2009]. This dominating influence motivates one to devise a more realistic model to better capture the physics of interface materials. The following are a few additional motivations to develop a more general interface model:

- increasing applications of thermal interfaces [Prasher 2006],
- unusual thermal behavior of surface and interfaces at the nanoscale [Berber et al. 2000; Che et al. 2000; Cahill et al. 2003; Prasher 2005],
- the study of interface mechanical characteristics by the vast majority of the literature is mainly based on cohesive zone models.

Keywords: thermomechanically energetic interfaces, interface elasticity, general imperfect interfaces, nonlocal damage, nanomaterials, finite element method.

Therefore, in this contribution, we follow the work of Javili et al. [2014] and Kaessmair et al. [2014], where the interface theory was extended to mechanically coherent energetic and thermally general imperfect (GI) interfaces. A thermally GI interface permits discontinuities in both temperature and normal heat flux. The extreme cases of thermally GI interfaces are highly conductive (HC) and lowly conductive (LC) interfaces, where the former allows a discontinuity in the normal heat flux but not in the temperature across the interface, and the latter permits a discontinuity in the temperature but not in the normal heat flux across the interface. Among the various thermal interfaces introduced above, an HC interface is termed thermally coherent due to the vanishing temperature jump. We point out that the thermally GI interface presented here may be specialized to all the other types of thermal interfaces. For further details on the different types of thermal imperfections, see [Esmaeili et al. 2016a; 2016b; Kaessmair et al. 2014; Javili et al. 2014] and references therein.

A mechanically coherent energetic interface is based on the *interface elasticity theory* proposed in [Gurtin and Murdoch 1975; Murdoch 1976]. Note that the coherence of the interface refers to the continuity in the displacement field across the interface. This manuscript is limited to mechanically coherent energetic interfaces. For further details, see, for instance, [Moeckel 1975; Daher and Maugin 1986; dell'Isola and Romano 1987; Gurtin 1998; Steigmann and Ogden 1999; Fried and Todres 2005; Fried and Gurtin 2007; Levitas and Javanbakht 2010; Javili and Steinmann 2010; Benveniste and Miloh 2001; Sharma et al. 2003; Dingreville et al. 2005; Duan et al. 2005a; 2005b; 2009; Benveniste 2013; Huang and Sun 2007; Fischer and Svoboda 2010; Yvonnet et al. 2011; Altenbach et al. 2012; Davydov et al. 2013] and the references therein. A restriction of the interface elasticity theory is that it only captures elastic interface behavior.

The nucleation of microvoids and strong discontinuities, such as cracks, can act as shields or amplify stress intensity in other regions of an interface. Consequently, this can influence the temperature distribution and thus the thermomechanical response of a body. Noting that the interface elasticity theory can only capture elastic behavior of energetic interfaces, the development of a more general interface model, in which interface inelasticity is taken into account, seems necessary.

Very recently in [Esmaeili et al. 2016a] we have considered thermally highly conductive (HC) interfaces in a thermomechanical body, whereby due to the highly conductive property the (otherwise mechanically coherent) interfaces allow for jumps in the normal heat flux. Moreover, they are equipped with interface stresses that are coupled to in-plane damage. In this contribution, we formulate a follow up version of [Esmaeili et al. 2016a] that generalizes the thermal part of the above interfaces to the thermally GI case, whereas the mechanical part is as before. Thereby this formulation embraces the two limiting cases of the previous HC interfaces (jump in normal heat flux) and the lowly conductive (LC) Kapitza interfaces, see [Esmaeili et al. 2016b], that allow for a jump in the temperature. Thus arbitrary combinations of HC and LC (jump in normal heat flux and jump in the temperature) are analyzed numerically.

To take into account the in-plane damage, a nonlocal continuum damage approach is utilized. For further details on this approach with application to bulk materials, see, for instance, [Kachanov 1958; Rabotnov 1963; Chaboche 1981; de Souza Neto and Perić 1996; de Souza Neto et al. 1998; Steinmann et al. 1994], among others. There are a few reasons to use a nonlocal damage model: first, mesh-objective finite element simulation of strain softening materials; second, determining the growth of microcracks by the energy release from the volume encompassing the microcrack [Bažant and Xi 1991]; third, the influence of the presence of a microcrack on the stress level of other neighboring microcracks; and finally

capturing size effects [Bažant and Jirásek 2002]. The nonlocality in this work is of integral-type, which then requires the use of an interactive (cut-off) radius, capturing size effects. The interactive radius is a function of the molecular structure of the intact material and the distribution and growth of the microcracks in the damaging material. It is not yet well-established how to determine the interactive radius from experiments (see [Bažant and Jirásek 2002] for further details). The degradation of the interface material here is measured using a tangential (in-plane) damage variable denoted by $\overline{D}_{\|}$. Consequently, as the damage variable evolves, all the mechanical and in-plane thermal properties of the interface are reduced. However, the out-of-plane thermal properties, i.e., the interface Kapitza resistance coefficient $\bar{r}_Q^0$ and the sensitivity $\bar{s}_0$, will increase as the damage evolves. The damage variable here is a function of the interface effective (undamaged) free energy $\overline{\Psi}^0$, which in turn depends on both the interface temperature $\overline{\Theta}$ and the interface deformation gradient $\overline{\boldsymbol{F}}$. Here, no distinction between thermal and mechanical damage has been made for the sake of simplicity and the fact that such distinction has not yet been physically motivated.

In summary, the key contributions of this work are as follows:

- To derive the governing equations of a thermomechanical solid possessing thermally GI and mechanically coherent energetic interface subject to in-plane degradation, within the fully nonlinear three dimensional setting.
- To present a thermodynamically consistent formulation and derive the dissipation inequality on the interface.
- To account for the effects of in-plane damage on the thermomechanical properties of the interface.
- To derive the thermal and mechanical weak forms.
- To derive the consistent tangent stiffness matrices in the bulk and on the interface.
- To present details of the computation of solids possessing thermally GI and mechanically coherent energetic interfaces within the three-dimensional, nonlinear and transient setting.
- To illustrate the theory with the help of numerical examples using the finite element method.

This paper is organized as follows. First the notation and certain key concepts are briefly introduced. Section 2 summarizes the kinematics of nonlinear continuum mechanics. The local governing equations, including the additional contributions from the interface, together with the constitutive relations are given in Section 3. A numerical framework for the interface is established in Section 4. The framework includes the weak formulation of the governing equations, the corresponding finite element implementation and the derivation of the consistent stiffness matrices. A series of numerical examples, based on the finite element approximation of the weak form, is presented in Section 5 to elucidate the theory. Section 6 concludes this work.

2. Problem definition

This section summarizes the kinematics of nonlinear continuum mechanics, including thermally general imperfect and mechanically coherent energetic interfaces and introduces the notation adopted here. Further details on the kinematics of deformable interfaces can be found in [Javili et al. 2013]. All over-lined

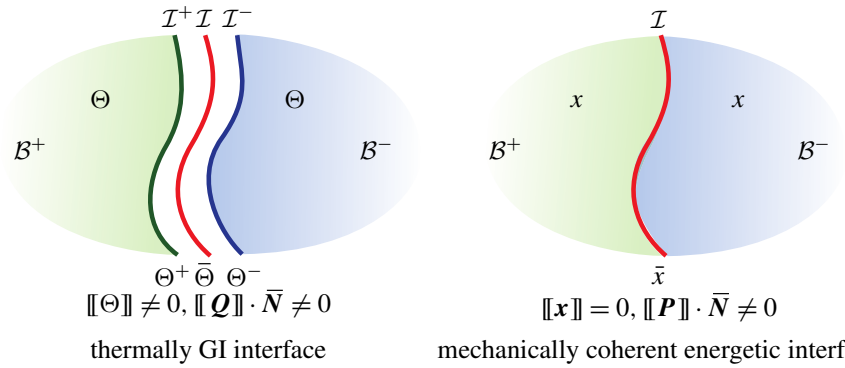

Figure 1. Thermally general imperfect interface, left, and mechanically coherent energetic interface, right. The interface in this work is mechanically coherent, thus no jump in deformation is allowed across the interface, $[\![\boldsymbol{\varphi}]\!] = \mathbb{0}$, $[\![\boldsymbol{x}]\!] = \mathbb{0}$, and energetic, thus the jump of the normal traction across the interface does not vanish, i.e., $[\![\boldsymbol{P}]\!] \cdot \bar{\boldsymbol{N}} \neq \mathbb{0}$. A thermally GI interface allows for the jump in temperature $[\![\Theta]\!] \neq \mathbb{0}$, and in normal heat flux $[\![\boldsymbol{Q}]\!] \cdot \bar{\boldsymbol{N}} \neq 0$ across the interface. The bulk and interface are denoted here by $\mathcal{B}$ and $\mathcal{I}$. The normal to the interface is denoted by $\bar{\boldsymbol{N}}$, see Figure 2. The in-plane degradation of the interface causes the degradation of mechanical and thermal properties of the interface through a tangential damage variable $\bar{D}_{\parallel}$.

quantities correspond to the interface.[1] The List of symbols gathers a list of notations frequently used in this manuscript.

Consider a continuum body $\mathcal{B}$ that takes the material configuration $\mathcal{B}_0 \subset \mathbb{E}^3$ at time $t = 0$, and the spatial configuration $\mathcal{B}_t$ at $t > 0$, as depicted in Figure 1. The body $\mathcal{B}$ is partitioned into two disjoint subdomains, $\mathcal{B}_0^+$ and $\mathcal{B}_0^-$, by an interface $\mathcal{I}_0$, thus the bulk is defined by $\mathcal{B}_0 := \mathcal{B}_0^+ \bigcup \mathcal{B}_0^-$, with reference placements of material particles labeled $\boldsymbol{X}$. The two sides of the interface $\mathcal{I}_0$ are denoted $\mathcal{I}_0^+ := \partial\mathcal{B}_0^+ \bigcap \mathcal{I}_0$ and $\mathcal{I}^- := \partial\mathcal{B}_0^- \bigcap \mathcal{I}_0$. The material particles on the interface are labeled $\bar{\boldsymbol{X}}$. The outward unit normal to $\partial\mathcal{B}_0$ is denoted $\boldsymbol{N}$. The outward unit normal to the boundary of the interface $\partial\mathcal{I}_0$, tangent to the interface $\mathcal{I}_0$, is denoted $\widetilde{\boldsymbol{N}}$. The unit normal to $\mathcal{I}_0$ is denoted $\bar{\boldsymbol{N}}$, whose direction is conventionally taken to point from the negative side of the interface to the positive side. The spatial counterparts of the various unit normals are $\boldsymbol{n}$, $\widetilde{\boldsymbol{n}}$ and $\bar{\boldsymbol{n}}$, respectively. The deformation maps of the bulk, and the negative and positive sides of the interface are denoted $\boldsymbol{\varphi}$, $\boldsymbol{\varphi}^-$ and $\boldsymbol{\varphi}^+$, respectively. The restriction of the motion $\boldsymbol{\varphi}$ to the interface is

[1] Direct notation is adopted throughout. Occasional use is made of index notation, the summation convention for repeated indices being implied. The three-dimensional Euclidean space is denoted by $\mathbb{E}^3$. The scalar product of two vectors $\boldsymbol{a}$ and $\boldsymbol{b}$ is denoted by $\boldsymbol{a} \cdot \boldsymbol{b} = [\boldsymbol{a}]_i [\boldsymbol{b}]_i$. The scalar product of two second-order tensors $\boldsymbol{A}$ and $\boldsymbol{B}$ is denoted by $\boldsymbol{A} : \boldsymbol{B} = [\boldsymbol{A}]_{ij} [\boldsymbol{B}]_{ij}$. The composition of two second-order tensors $\boldsymbol{A}$ and $\boldsymbol{B}$, denoted by $\boldsymbol{A} \cdot \boldsymbol{B}$, is a second-order tensor with coefficients $[\boldsymbol{A} \cdot \boldsymbol{B}]_{ij} = [\boldsymbol{A}]_{im} [\boldsymbol{B}]_{mj}$. The nonstandard products of a fourth-order tensor $\mathbb{C}$ and a vector $\boldsymbol{b}$ is defined by $[\boldsymbol{b} \cdot \mathbb{C}]_{ikl} = [\mathbb{C}]_{ijkl} [\boldsymbol{b}]_j$. The action of a second-order tensor $\boldsymbol{A}$ on a vector $\boldsymbol{a}$ is given by $[\boldsymbol{A} \cdot \boldsymbol{a}]_i = [\boldsymbol{A}]_{ij} [\boldsymbol{a}]_j$. The standard product of a fourth-order tensor $\mathbb{C}$ and a second-order tensor $\boldsymbol{A}$ is defined by $[\mathbb{C} : \boldsymbol{A}]_{ij} = [\mathbb{C}]_{ijkl} [\boldsymbol{A}]_{kl}$. The dyadic product of two vectors $\boldsymbol{a}$ and $\boldsymbol{b}$ is a second-order tensor $\boldsymbol{D} = \boldsymbol{a} \otimes \boldsymbol{b}$ with $[\boldsymbol{D}]_{ij} = [\boldsymbol{a}]_i [\boldsymbol{b}]_j$. Two nonstandard dyadic products of two second-order tensors $\boldsymbol{A}$ and $\boldsymbol{B}$ are the fourth-order tensors $[\boldsymbol{A} \overline{\otimes} \boldsymbol{B}]_{ijkl} = [\boldsymbol{A}]_{ik} [\boldsymbol{B}]_{jl}$ and $[\boldsymbol{A} \underline{\otimes} \boldsymbol{B}]_{ijkl} = [\boldsymbol{A}]_{il} [\boldsymbol{B}]_{jk}$. The average and jump of a quantity $\{\bullet\}$ over an interface are defined by $\{\!\{\bullet\}\!\} = \frac{1}{2}[\{\bullet\}^+ + \{\bullet\}^-]$ and $[\![\{\bullet\}]\!] = \{\bullet\}^+ - \{\bullet\}^-$, respectively.

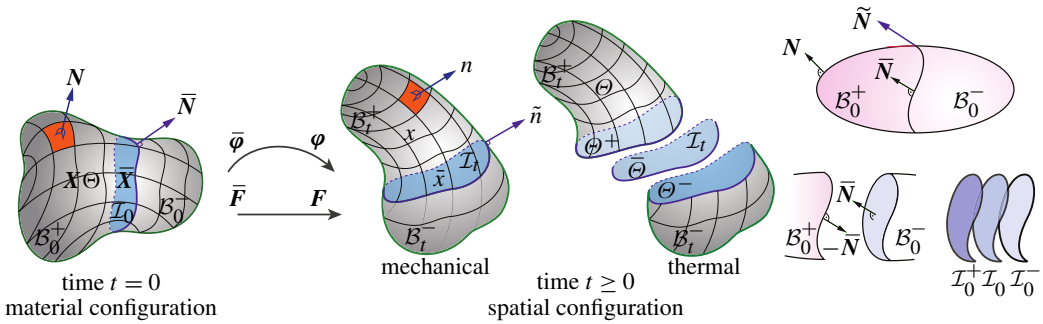

Figure 2. The bulk domain $\mathcal{B}_0$, the bulk subdomains $\mathcal{B}_0^{\pm}$, the interface $\mathcal{I}_0$, the two sides of the interface $\mathcal{I}_0^{\pm}$ and the unit normals to the surface $\boldsymbol{N}$, the interface $\overline{\boldsymbol{N}}$, and boundary of the interface $\widetilde{\boldsymbol{N}}$, all defined in the material configuration. The bulk, interface and the two sides of interface deformation maps, denoted as $\boldsymbol{\varphi}$, $\overline{\boldsymbol{\varphi}}$ and $\boldsymbol{\varphi}^{\pm}$, respectively, map the material configuration to the spatial configuration at time t. The bulk domain $\mathcal{B}_t$, the bulk subdomains $\mathcal{B}_t^{\pm}$, the interface $\mathcal{I}_t$ and its two sides $\mathcal{I}_t^{\pm}$, the unit normals to the surface $\boldsymbol{n}$, interface $\overline{\boldsymbol{n}}$, and boundary of the interface $\widetilde{\boldsymbol{n}}$, all defined in the spatial configuration. The bulk temperatures on plus and minus side of the interface and the interface temperature are denoted by Θ^+, Θ^- and $\overline{\Theta}$, respectively. The interface unit normal is pointing from the negative side of the interface to the positive side. The bulk and (rank-deficient) interface deformation gradients are $\boldsymbol{F}$ and $\overline{\boldsymbol{F}}$, respectively. The interface is mechanically coherent and thermally noncoherent.

defined by $\overline{\boldsymbol{\varphi}}$. The current placements of particles in the bulk and on the two sides of the interface are denoted $\boldsymbol{x}$ and $\boldsymbol{x}^{\mp}$ where the spatial placement of particles on the interface are designated as $\bar{\boldsymbol{x}}$. One should note that $\boldsymbol{\varphi}^+ = \boldsymbol{\varphi}^- = \overline{\boldsymbol{\varphi}}$ and $\boldsymbol{x}^+ = \boldsymbol{x}^- = \bar{\boldsymbol{x}}$ for mechanically coherent interfaces. This means the interface placement is always between the two lateral sides of the interface. The interface and bulk temperature on two sides of the interface are denoted by $\overline{\Theta}$, Θ^+ and Θ^-, respectively.

Remark 1. Since the interface is thermally general imperfect, the bulk temperatures Θ^+ and Θ^- can differ from each other. This is in contrast with a highly conductive interface where the jump of temperature across the interface vanishes and thus $\overline{\Theta} = \Theta^+ = \Theta^-$. Moreover, on a thermally general imperfect interface, the relation between the bulk and the interface temperature $\overline{\Theta}$ is (in general) unknown. In other words, the interface temperature does not necessarily take a value between the bulk temperatures on the two sides of the interface (for further details, see [Javili et al. 2014; Esmaeili et al. 2016a]).

The bulk and the (rank-deficient) interface deformation gradients $\boldsymbol{F}$ and $\overline{\boldsymbol{F}}$, together with the corresponding velocities $\boldsymbol{V}$ and $\overline{\boldsymbol{V}}$ are respectively defined by

$$\boldsymbol{F}(\boldsymbol{X},t) := \operatorname{Grad}\boldsymbol{\varphi}(\boldsymbol{X},t), \quad \boldsymbol{V} := \mathrm{D}_t\boldsymbol{\varphi}(\boldsymbol{X},t) \quad \text{and} \quad \overline{\boldsymbol{F}}(\overline{\boldsymbol{X}},t) := \overline{\operatorname{Grad}}\,\overline{\boldsymbol{\varphi}}(\overline{\boldsymbol{X}},t), \quad \overline{\boldsymbol{V}} := \mathrm{D}_t\overline{\boldsymbol{\varphi}}(\overline{\boldsymbol{X}},t). \tag{1}$$

Thereby the interface gradient and divergence operators respectively read

$$\overline{\operatorname{Grad}}\{\dot{\bullet}\} := \operatorname{Grad}\{\dot{\bullet}\}\cdot\bar{\boldsymbol{I}} \quad \text{and} \quad \overline{\operatorname{Div}}\{\dot{\bullet}\} := \overline{\operatorname{Grad}}\{\dot{\bullet}\}:\bar{\boldsymbol{I}} \quad \text{with} \quad \bar{\boldsymbol{I}} := \boldsymbol{I} - \overline{\boldsymbol{N}}\otimes\overline{\boldsymbol{N}}, \tag{2}$$

where $\bar{\boldsymbol{I}}$ and $\boldsymbol{I}$ denote the interface and bulk unit tensors. Their spatial counterparts are denoted $\bar{\boldsymbol{i}}$ and $\boldsymbol{i}$. Finally the bulk and interface Jacobians are denoted by

$$J := \det \boldsymbol{F} > 0 \quad \text{and} \quad \bar{J} := \overline{\det}\ \bar{\boldsymbol{F}} > 0,$$

respectively, with $\overline{\det}\{\bullet\}$ denoting the area determinant [Steinmann 2008].

3. Governing equations

The local balance equations of force, energy and entropy in the bulk and on the interface together with the associated boundary conditions are listed in Table 1 (for further details, see [Esmaeili et al. 2016a]). The considered interface model deals with interfaces that are

- mechanically coherent, $[\![\boldsymbol{\varphi}]\!] = \mathbb{0}$,
- mechanically energetic, thus $[\![\boldsymbol{P}]\!] \cdot \bar{\boldsymbol{N}} \neq \mathbb{0}$ and
- thermally general imperfect, $[\![\boldsymbol{Q}]\!] \cdot \bar{\boldsymbol{N}} \neq 0$ and $[\![\Theta]\!] \neq 0$.

The third property, i.e., thermal general imperfection of the interface, is characterized by allowing a jump both in the temperature and the normal heat flux ($[\![\Theta]\!] \neq 0$ and $[\![\boldsymbol{Q}]\!] \cdot \bar{\boldsymbol{N}} \neq 0$, respectively) across the interface. Also note that a thermally GI interface is fully dissipative. See Section 3 for further elaborations.

Remark 2. In what follows we briefly discuss different kinds of thermal interfaces:

force balance:	$\operatorname{Div}\boldsymbol{P} + \boldsymbol{B}^{\mathrm{p}} = \mathbb{0}$	in $\mathcal{B}_0$	$\widehat{\boldsymbol{B}}^{\mathrm{p}} = \boldsymbol{P}\cdot\boldsymbol{N}$	on $\partial\mathcal{B}_0^{\mathrm{N}}$
	$\overline{\operatorname{Div}}\,\bar{\boldsymbol{P}} + \bar{\boldsymbol{B}}^{\mathrm{p}} = -[\![\boldsymbol{P}]\!]\cdot\bar{\boldsymbol{N}}$	on $\mathcal{I}_0$	$\widetilde{\boldsymbol{B}}^{\mathrm{p}} = \bar{\boldsymbol{P}}\cdot\widetilde{\boldsymbol{N}}$	on $\partial\mathcal{I}_0^{\mathrm{N}}$
energy:	$-\boldsymbol{P} : \operatorname{Grad}\boldsymbol{V} + \operatorname{Div}\boldsymbol{Q} - Q^{\mathrm{p}} + \mathrm{D}_t\mathcal{E} = 0$	in $\mathcal{B}_0$	$\widehat{Q}^{\mathrm{p}} = -\boldsymbol{Q}\cdot\boldsymbol{N}$	on $\partial\mathcal{B}_0^{\mathrm{N}}$
	$-\bar{\boldsymbol{P}} : \overline{\operatorname{Grad}}\,\bar{\boldsymbol{V}} + \overline{\operatorname{Div}}\,\bar{\boldsymbol{Q}} - \bar{Q}^{\mathrm{p}} + \mathrm{D}_t\bar{\mathcal{E}} = -[\![\boldsymbol{Q}]\!]\cdot\bar{\boldsymbol{N}}$	on $\mathcal{I}_0$		
entropy:	$\operatorname{Div}\boldsymbol{H} - H^{\mathrm{p}} + \mathrm{D}_t\Xi \geq 0$	in $\mathcal{B}_0$	$\widehat{H}^{\mathrm{p}} = -\boldsymbol{H}\cdot\boldsymbol{N}$	on $\partial\mathcal{B}_0^{\mathrm{N}}$
	$\overline{\operatorname{Div}}\,\bar{\boldsymbol{H}} - \bar{H}^{\mathrm{p}} + \mathrm{D}_t\bar{\Xi} \geq -[\![\boldsymbol{H}]\!]\cdot\bar{\boldsymbol{N}}$	on $\mathcal{I}_0$	$\widetilde{H}^{\mathrm{p}} = -\bar{\boldsymbol{H}}\cdot\widetilde{\boldsymbol{N}}$	on $\partial\mathcal{I}_0^{\mathrm{N}}$

$\boldsymbol{B}^{\mathrm{p}}$	force vector per unit volume	$\widehat{\boldsymbol{B}}^{\mathrm{p}}$	surface traction per unit area
$\bar{\boldsymbol{B}}^{\mathrm{p}}$	force vector per unit area	$\widetilde{\boldsymbol{B}}^{\mathrm{p}}$	curve traction per unit length
$\boldsymbol{Q}$	bulk heat flux vector per unit area	$\bar{\boldsymbol{Q}}$	interface heat flux vector per unit length
$\boldsymbol{H}$	bulk entropy flux vector per unit area	$\bar{\boldsymbol{H}}$	interface entropy flux vector per unit length
Q^{p}	bulk heat source per unit volume	$\widehat{Q}^{\mathrm{p}}$	surface heat source per unit area
$\bar{Q}^{\mathrm{p}}$	interface heat source per unit area	$\widetilde{Q}^{\mathrm{p}}$	curve heat source per unit length
H^{p}	bulk entropy source per unit volume	$\widehat{H}^{\mathrm{p}}$	surface entropy source per unit area
$\bar{H}^{\mathrm{p}}$	interface entropy source per unit area	$\widetilde{H}^{\mathrm{p}}$	curve entropy source per unit length
$\mathcal{E}$	bulk internal energy per unit volume	$\bar{\mathcal{E}}$	interface internal energy per unit area

Table 1. Localized force, energy and entropy balances in the bulk and on the interface in the material configuration. The notation $\{\bullet\}^{\mathrm{p}}$ is to denote prescribed quantities. Balance of angular momentum results in the symmetry of the bulk Cauchy stress, i.e., $\boldsymbol{P}\cdot\boldsymbol{F}^t = \boldsymbol{F}\cdot\boldsymbol{P}^t$, and the interface Cauchy stress, i.e., $\bar{\boldsymbol{P}}\cdot\bar{\boldsymbol{F}}^t = \bar{\boldsymbol{F}}\cdot\bar{\boldsymbol{P}}^t$, in the material configuration.

- A thermally perfect interface is recovered when $[\![\boldsymbol{Q}]\!]\cdot\overline{\boldsymbol{N}}=0$ and $[\![\Theta]\!]=0$.
- A highly conductive interface imposes a vanishing temperature jump across the interface while allowing for the jump of normal heat flux across the interface, i.e., $[\![\Theta]\!]=0$ and $[\![\boldsymbol{Q}]\!]\cdot\overline{\boldsymbol{N}}\neq 0$. Note that a continuous temperature distribution across the interface does not necessary imply a HC interface (see [Javili et al. 2014] for further details). Furthermore, an HC interface is nondissipative due to the vanishing temperature jump across the interface, which results in the interface temperature being identical to the bulk temperatures on the two sides of the interface.
- A lowly conductive (LC) interface allows for a temperature jump but not for a jump in the normal heat flux across the interface, i.e., $[\![\Theta]\!]\neq 0$ and $[\![\boldsymbol{Q}]\!]\cdot\overline{\boldsymbol{N}}=0$. This model is subject to Kapitza's assumption of thermal resistance. Note that an LC interface is semidissipative (possessing only one dissipation contribution, see Section 3 for further discussions). For this interface, a connection between the interface and the bulk temperature (in general) can not be drawn.
- A semidissipative (SD) interface is a generalization of the LC interface so that the jump in both the temperature and the normal heat flux is admissible, i.e., $[\![\boldsymbol{Q}]\!]\cdot\overline{\boldsymbol{N}}\neq 0$ and $[\![\Theta]\!]\neq 0$. Analogous to the LC interface, the same dissipation contribution is nonvanishing for an SD interface. However, unlike an LC interface, the SD interface imposes a relation between the interface and the bulk temperature, or more precisely between what we call interface and bulk coldness. The coldness here is defined as the inverse of the temperature.
- A fully dissipative (FD) interface is a GI interface similar to an SD interface in the sense that both $[\![\boldsymbol{Q}]\!]\cdot\overline{\boldsymbol{N}}\neq 0$ and $[\![\Theta]\!]\neq 0$ are admissible. Nonetheless, an FD interface is generalized to possess two dissipation contributions. Consequently, a relation (in general) between interface and bulk temperature cannot be established (analogously to an LC interface). Additionally, for an FD interface, the interface temperature shall be considered as an independent degree of freedom.

Furthermore, both thermal and mechanical properties of the interface are affected by the interface in-plane degradation. In doing so, a reduction factor $[1-\overline{D}_{\parallel}]$ is introduced, which reduces the mechanical and in-plane thermal properties of the interface as the damage $\overline{D}_{\parallel}$ evolves. The out-of-plane thermal properties of the interface, the sensitivity $\bar{s}_0$ and the Kapitza thermal resistance $\bar{r}_Q^0$, are inversely affected by the reduction factor, i.e., $\bar{s}=\bar{s}_0/[1-\overline{D}_{\parallel}]$ and $\bar{r}_Q=\bar{r}_Q^0/[1-\overline{D}_{\parallel}]$. Note that in this work the damage variable is a function of the nonlocal equivalent distortion $\overline{F}_{\text{nloc}}$, which in turn depends on the interface deformation gradient $\overline{\boldsymbol{F}}$ and temperature $\overline{\Theta}$. The interface Piola stress $\overline{\boldsymbol{P}}$ is a superficial tensor field possessing the property $\overline{\boldsymbol{P}}\cdot\overline{\boldsymbol{N}}=\mathbb{0}$. It is noteworthy to mention that the interface is mechanically coherent and, due to the interface energetics, a discontinuity in the traction across the interface is allowed and hence $[\![\boldsymbol{P}]\!]\cdot\overline{\boldsymbol{N}}\neq\mathbb{0}$.

Next are the bulk and interface free energies. The corresponding constitutive relations and temperature evolution equations are given in Table 2. Note that $0\leq\overline{D}_{\parallel}(\overline{\boldsymbol{F}},\overline{\Theta})\leq 1$ and $\bar{\vartheta}$ is an internal variable; $\boldsymbol{k}$ and $\bar{\boldsymbol{k}}_0$ denote the bulk and interface positive (semi) definite thermal conductivity tensors. For thermally isotropic materials in the spatial configuration, $\boldsymbol{k}=k\boldsymbol{i}$ and $\bar{\boldsymbol{k}}_0=\bar{k}_0\bar{\boldsymbol{i}}$, where the scalars $k\geq 0$ and $\bar{k}_0\geq 0$ are the thermal conductivity coefficients in the bulk and on the interface, respectively. The heat capacity coefficients in the bulk and on the interface are denoted by $c_{\boldsymbol{F}}$ and $\bar{c}_{\overline{\boldsymbol{F}}}=[1-\overline{D}_{\parallel}]\bar{c}^0_{\overline{\boldsymbol{F}}}$, where $\bar{c}^0_{\overline{\boldsymbol{F}}}$ is the interface heat capacity coefficient associated with the undamaged (virgin) state of the interface material.

free energy:	$\Psi \equiv \Psi(\boldsymbol{F}, \Theta)$ $\overline{\Psi} \equiv \overline{\Psi}(\overline{\boldsymbol{F}}, \overline{\Theta}, \overline{D}_{\parallel}, \bar{\vartheta}) = [1-\overline{D}_{\parallel}]\overline{\Psi}^0$	in $\mathcal{B}_0$ on $\mathcal{I}_0$
constitutive relations:	$\boldsymbol{P} := \partial\Psi/\partial\boldsymbol{F}$ and $\Xi := -\partial\Psi/\partial\Theta$ $\overline{\boldsymbol{P}} := \partial\overline{\Psi}/\partial\overline{\boldsymbol{F}} = [1-\overline{D}_{\parallel}]\overline{\boldsymbol{P}}_0$ and $\overline{\Xi} := -\partial\overline{\Psi}/\partial\overline{\Theta} = [1-\overline{D}_{\parallel}]\overline{\Xi}^0$ $\boldsymbol{Q} = -J\boldsymbol{F}^{-1}\cdot\boldsymbol{k}\cdot\boldsymbol{F}^{-\mathrm{t}}\cdot\mathrm{Grad}\,\Theta$ $\overline{\boldsymbol{Q}} = -\overline{J}\overline{\boldsymbol{F}}^{-1}\cdot[1-\overline{D}_{\parallel}]\bar{\boldsymbol{k}}_0\cdot\overline{\boldsymbol{F}}^{-\mathrm{t}}\cdot\overline{\mathrm{Grad}}\,\overline{\Theta}$	in $\mathcal{B}_0$ on $\mathcal{I}_0$ in $\mathcal{B}_0$ on $\mathcal{I}_0$
temperature evolution:	$c_{\boldsymbol{F}}\mathrm{D}_t\Theta = -\mathrm{Div}\,\boldsymbol{Q} + \Theta\partial_\Theta\boldsymbol{P} : \mathrm{D}_t\boldsymbol{F} + Q^{\mathrm{p}}$ with $c_{\boldsymbol{F}} := -\Theta\partial^2\Psi/\partial\Theta^2$ $\bar{c}_{\overline{\boldsymbol{F}}}\mathrm{D}_t\overline{\Theta} = -\overline{\mathrm{Div}}\;\overline{\boldsymbol{Q}} + \overline{\Theta}\partial_{\overline{\Theta}}\overline{\boldsymbol{P}} : \mathrm{D}_t\overline{\boldsymbol{F}} + \overline{Q}^{\mathrm{p}} - [\![\boldsymbol{Q}]\!]\cdot\overline{\boldsymbol{N}}$ with $\bar{c}_{\overline{\boldsymbol{F}}} := -[1-\overline{D}_{\parallel}]\overline{\Theta}\partial^2\overline{\Psi}^0/\partial\overline{\Theta}^2$	in $\mathcal{B}_0^{\mathrm{N}}$ on $\mathcal{I}_0^{\mathrm{N}}$

Table 2. Bulk and interface free energies, the corresponding constitutive relations and temperature evolution equations.

To proceed, a Helmholtz energy[2] is considered for the interface containing the following arguments [Esmaeili et al. 2016a]:

$$\overline{\Psi}(\overline{\boldsymbol{F}}, \overline{\Theta}, \overline{D}, \bar{\vartheta}) = [1-\overline{D}]\overline{\Psi}_0(\overline{\boldsymbol{F}}, \overline{\Theta}) + \int_0^{\bar{\vartheta}} \overline{\mathcal{H}}(\bar{\vartheta}^*)\,\mathrm{d}\bar{\vartheta}^*, \tag{3}$$

where $\overline{\mathcal{H}}(\bar{\vartheta})$ denotes a monotonically increasing function depending on the internal variable $\bar{\vartheta}$. Now by differentiating (3) with respect to time, particularizing the Clausius–Plank inequality and making use of the constitutive relations, one expresses the interface reduced dissipation $\overline{\mathcal{D}}_{\mathrm{red}}$ as (for further details, see [Esmaeili et al. 2016a])

$$\overline{\mathcal{D}}_{\mathrm{red}} = \underbrace{\overline{Y}\dot{\overline{D}}_{\parallel} - \overline{\mathcal{H}}(\bar{\vartheta})\dot{\bar{\vartheta}}}_{\overline{\mathcal{D}}_{\parallel}} + \underbrace{\overline{\Theta}\big[[\![\Theta^{-1}]\!]\{\!\{\boldsymbol{Q}\}\!\} - \big[\overline{\Theta}^{-1} - \{\!\{\Theta^{-1}\}\!\}\big][\![\boldsymbol{Q}]\!]\cdot\overline{\boldsymbol{N}}}_{\overline{\mathcal{D}}_{\nparallel}} \geq 0 \text{ with } \overline{Y} = \overline{\Psi}^0(\overline{\boldsymbol{F}}, \overline{\Theta}) = -\frac{\partial\overline{\Psi}}{\partial\overline{D}_{\parallel}}, \tag{4}$$

where the quantity $\overline{Y}$ is the thermodynamic force conjugate to the interface damage variable $\overline{D}_{\parallel}$. Next, together with satisfying $\overline{\mathcal{D}}_{\parallel} \geq 0$, a damage condition $\overline{\Upsilon}$ is introduced as [Steinmann 1999]

$$\overline{\Upsilon}(\overline{Y},\ \overline{\mathcal{H}}) = \bar{\upsilon}(\overline{Y}) - \overline{\mathcal{H}}(\bar{\vartheta}) \leq 0, \tag{5}$$

with $\bar{\upsilon}$ being a monotonically increasing function. The damage evolution law and the Kuhn–Tucker conditions can be obtained from the postulate of maximum dissipation using the Lagrange-multiplier method. Now by choosing $\bar{\upsilon}(\bullet) = \overline{\mathcal{H}}(\bullet)$, and defining the change of variables $\overline{F}_{\max} := f(\bar{\vartheta})$ and $\overline{F}_{\mathrm{nloc}} := f(\overline{Y})$ and assuming f to be a monotonically increasing function with the property $f(0) = 0$, an alternative damage condition to (5) takes the form extended to integral-type nonlocality [Esmaeili et al. 2016a]:

$$\bar{\phi}(\overline{F}_{\mathrm{nloc}}, \overline{F}_{\max}) = \overline{F}_{\mathrm{nloc}} - \overline{F}_{\max} \leq 0,\ \text{ with } \overline{F}_{\mathrm{nloc}}(\bar{\boldsymbol{x}}_{\mathrm{r}}) = \int_{\mathcal{I}_0} \bar{\omega}(\bar{\boldsymbol{x}}_{\mathrm{r}}, \bar{\boldsymbol{x}}_{\mathrm{s}})\overline{F}_{\mathrm{loc}}(\boldsymbol{x}_s)\,\mathrm{d}A \text{ and } \overline{F}_{\mathrm{loc}} := \sqrt{\frac{2\overline{Y}}{\overline{E}}}, \tag{6}$$

[2]The integral term in (3) is introduced in analogy with that of [Simo and Hughes 1998, §1.3.3] and is the energy storage in the material due to the accumulation of microscopic defects.

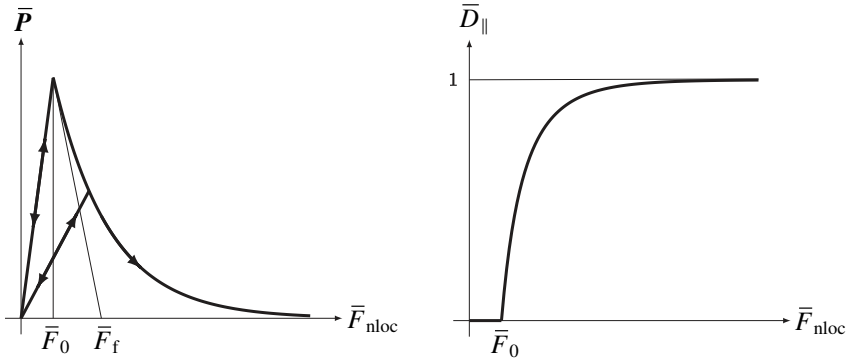

Figure 3. Stress vs. nonlocal equivalent distortion with exponential softening on the interface, left. Damage variable vs. nonlocal equivalent distortion associated with (8), right. The parameters $\bar{F}_0$ and $\bar{F}_{\mathrm{f}}$ are the interface critical equivalent distortion and ductility response.

where $\bar{F}_{\max}(t) = \max_{s\in[0,\,t]}\{\bar{F}_0, \bar{F}_{\mathrm{nloc}}|_s\}$, $\bar{F}_0$ is the damage threshold, $\bar{F}_{\mathrm{loc}}$ is the local equivalent distortion, and $\bar{E}$ is the interface Young's modulus. Note that the damage variable is eventually simply a function of $\bar{F}_{\max}$, i.e., $\bar{D}_{\|} = \bar{\mathcal{D}}_{\|}(\bar{F}_{\max})$. In $(6)_2$, $\bar{\omega}(\bar{\boldsymbol{x}}_{\mathrm{r}},\ \bar{\boldsymbol{x}}_{\mathrm{s}})$ is a given nonlocal weight function depending on the geodesic distance $\bar{r} = \|\bar{\boldsymbol{x}}_{\mathrm{r}} - \bar{\boldsymbol{x}}_{\mathrm{s}}\|_{\mathcal{I}}$ between the source point $\bar{\boldsymbol{x}}_{\mathrm{s}}$ and the receiver point $\bar{\boldsymbol{x}}_{\mathrm{r}}$. On the interface, the weight function $\bar{\omega}$ here is defined as

$$\bar{\omega}(\bar{\boldsymbol{x}}_{\mathrm{r}}, \bar{\boldsymbol{x}}_{\mathrm{s}}) = \frac{\bar{\omega}_0(\bar{r})}{\int_{\mathcal{I}_0} \bar{\omega}_0(\bar{r})\,\mathrm{d}A} \quad \text{with} \quad \bar{\omega}_0(\bar{r}) = \begin{cases} [1 - \bar{r}^2/\bar{R}^2]^2 & \text{if } |\bar{r}| \le \bar{R}, \\ 0 & \text{if } |\bar{r}| \ge \bar{R}, \end{cases} \tag{7}$$

where $\bar{\omega}_0(\bar{r})$ is a nonnegative and monotonically decreasing (for $\bar{r} \ge 0$) piecewise polynomial bell-shaped function. The interface interaction radius is denoted by $\bar{R}$. The damage function, relating $\bar{D}_{\|}$ to the history variable $\bar{F}_{\max}$, is given as follows (see Figure 3, right):

$$\bar{D}_{\|} = \bar{\mathcal{D}}_{\|}(\bar{F}_{\max}) = \begin{cases} 0 & \text{if } \bar{F}_{\max} \le \bar{F}_0, \\ 1 - \dfrac{\bar{F}_0}{\bar{F}_{\max}} \exp\left(-\dfrac{\bar{F}_{\max} - \bar{F}_0}{\bar{F}_{\mathrm{f}} - \bar{F}_0}\right) & \text{if } \bar{F}_{\max} \ge \bar{F}_0, \end{cases} \tag{8}$$

where $\bar{F}_{\mathrm{f}}$ affects the ductility of the response. An illustration is depicted in Figure 3, left.

To satisfy $\bar{\mathcal{D}}_{\shortparallel} \ge 0$ in $(4)_1$, using the relation $[\![\Theta^{-1}]\!] = -[\![\Theta]\!]\{\!\{\Theta^{-1}\}\!\}\{\!\{\Theta\}\!\}^{-1}$, we enforce the fulfillment of the following two conditions:

$$^1\bar{\mathcal{D}}_{\shortparallel} = -[\![\Theta]\!]\{\!\{\boldsymbol{Q}\}\!\} \cdot \bar{\boldsymbol{N}} \ge 0 \quad \text{and} \quad ^2\bar{\mathcal{D}}_{\shortparallel} = -[\bar{\Theta}^{-1} - \{\!\{\Theta^{-1}\}\!\}][\![\boldsymbol{Q}]\!] \cdot \bar{\boldsymbol{N}} \ge 0. \tag{9}$$

Remark 3. For the interface considered here, both dissipation contributions in (9) are positive and hence the interface is termed fully dissipative. For an HC interface, both of these dissipation contributions vanish since $[\![\Theta]\!] = 0$. Both SD and LC interfaces allow for $^1\bar{\mathcal{D}}_{\shortparallel}$ to be nonzero since $[\![\Theta]\!] \ne 0$. The difference is that for an SD interface $[\![\boldsymbol{Q}]\!] \cdot \bar{\boldsymbol{N}} \ne 0$ and $[\bar{\Theta}^{-1} - \{\!\{\Theta^{-1}\}\!\}] = 0$, whereas for an LC interface $[\![\boldsymbol{Q}]\!] \cdot \bar{\boldsymbol{N}} = 0$ and a relation between the interface and the bulk temperatures is (in general) unknown (see also Remark 2).

To this end, Fourier-like relations are introduced as follows:

$$[\![\Theta]\!] = -\frac{\bar{r}_Q^0}{[1-\overline{D}_\parallel]}\{\!\{\boldsymbol{Q}\}\!\}\cdot\overline{\boldsymbol{N}} \quad \text{and} \quad \overline{\Theta}^{-1} - \{\!\{\Theta^{-1}\}\!\} = -\frac{\bar{s}_0}{[1-\overline{D}_\parallel]}[\![\boldsymbol{Q}]\!]\cdot\overline{\boldsymbol{N}}, \tag{10}$$

where $\bar{r}_Q^0 \geq 0$ and $\bar{s}_0 \geq 0$ are the undamaged (virgin) Kapitza resistance coefficient and the thermal sensitivity, respectively. As the interface damage grows and thus the reduction factor $[1-D_\parallel]$ decreases, one expects a more pronounced jump in the temperature across the interface and a less strong coupling between the bulk and the interface temperatures due to $\bar{r}_Q^0/[1-\overline{D}_\parallel]$ and $\bar{s}_0/[1-\overline{D}_\parallel]$ taking higher values. This observation is illustrated by the numerical results, which will be presented later.

4. Computational framework

Here we establish a numerical framework that encompasses thermohyperelasticity combined with a nonlocal damage model on the thermally general imperfect (GI) and mechanically coherent energetic interface. The weak form, together with its temporal and spatial discretizations, will be presented next.

The localized force balance equations in the bulk and on the interface given in Table 1 are tested with vector valued test functions $\delta\boldsymbol{\varphi} \in \mathscr{H}^1(\mathcal{B}_0)$ and $\delta\overline{\boldsymbol{\varphi}} \in \mathscr{H}^1(\mathcal{I}_0)$, respectively. By integrating the result over all domains in the material configuration, using the bulk and interface divergence theorems and the superficiality properties of the interface Piola stress, the weak form of the balance of linear momentum reads

$$\begin{aligned}
&\int_{\mathcal{B}_0} \boldsymbol{P} : \operatorname{Grad}\delta\boldsymbol{\varphi}\,\mathrm{d}V + \int_{\mathcal{I}_0}[1-\overline{D}_\parallel]\,\overline{\boldsymbol{P}}_0 : \overline{\operatorname{Grad}}\,\delta\overline{\boldsymbol{\varphi}}\,\mathrm{d}A - \int_{\mathcal{B}_0}\delta\boldsymbol{\varphi}\cdot\boldsymbol{B}^{\mathrm{p}}\,\mathrm{d}V - \int_{\mathcal{I}_0}\delta\overline{\boldsymbol{\varphi}}\cdot\overline{\boldsymbol{B}}^{\mathrm{p}}\,\mathrm{d}A - \int_{\partial\mathcal{B}_0^{\mathrm{N}}}\delta\boldsymbol{\varphi}\cdot\widehat{\boldsymbol{B}}_{\mathrm{N}}^{\mathrm{p}}\,\mathrm{d}A \\
&- \int_{\partial\mathcal{I}_0^{\mathrm{N}}}\delta\overline{\boldsymbol{\varphi}}\cdot\widetilde{\boldsymbol{B}}_{\mathrm{N}}^{\mathrm{p}}\,\mathrm{d}L = 0, \quad \forall\delta\boldsymbol{\varphi}\in\mathscr{H}^1(\mathcal{B}_0) \text{ and } \forall\delta\overline{\boldsymbol{\varphi}}\in\mathscr{H}^1(\mathcal{I}_0) \quad \text{with} \quad \delta\overline{\boldsymbol{\varphi}} = \{\!\{\delta\boldsymbol{\varphi}\}\!\}|_{\mathcal{I}_0} \text{ and } [\![\delta\boldsymbol{\varphi}]\!] = \mathbb{0}.
\end{aligned} \tag{11}$$

Analogously, the thermal weak form is derived first by testing the local temperature evolutions (see Table 2) in the bulk and on the interface with the scalar-valued test function $\delta\Theta \in \mathscr{H}_0^1(\mathcal{B}_0)$ and $\delta\overline{\Theta} \in \mathscr{H}_0^1(\mathcal{I}_0)$, respectively. The result is then integrated over the corresponding domains in the material configuration, resulting in the global weak form of the temperature evolution equation as follows:

$$\begin{aligned}
&\int_{\mathcal{B}_0} \boldsymbol{Q}\cdot\operatorname{Grad}\delta\Theta - \delta\Theta c_{\boldsymbol{F}}\mathrm{D}_t\Theta + \delta\Theta\,Q^{\mathrm{p}} + \delta\Theta\Theta\,\partial_\Theta\boldsymbol{P} : \mathrm{D}_t\boldsymbol{F}\,\mathrm{d}V + \int_{\partial\mathcal{B}_0^{\mathrm{N}}}\delta\Theta\,\widehat{Q}_{\mathrm{N}}^{\mathrm{p}}\,\mathrm{d}A \\
&+ \int_{\mathcal{I}_0}[1-\overline{D}_\parallel]\,\overline{\boldsymbol{Q}}_0\cdot\overline{\operatorname{Grad}}\,\delta\overline{\Theta} - \delta\overline{\Theta}[1-\overline{D}_\parallel]\bar{c}_{\overline{\boldsymbol{F}}}^0\mathrm{D}_t\overline{\Theta} + \delta\overline{\Theta}\,\overline{Q}^{\mathrm{p}} + \delta\overline{\Theta}\overline{\Theta}\big[[1-\overline{D}_\parallel]\partial_{\overline{\Theta}}\overline{\boldsymbol{P}}_0 - \partial_{\overline{\Theta}}\overline{\mathbb{D}}_\parallel\,\overline{\boldsymbol{P}}_0\big] : \mathrm{D}_t\overline{\boldsymbol{F}}\,\mathrm{d}A \\
&- \int_{\mathcal{I}_0}[\![\delta\Theta]\!][1-\overline{D}_\parallel]\frac{1}{\bar{r}_Q^0}[\![\Theta]\!] - [\delta\overline{\Theta} - \{\!\{\delta\Theta\}\!\}][1-\overline{D}_\parallel]\frac{1}{\bar{s}_0}[\overline{\Theta}^{-1} - \{\!\{\Theta^{-1}\}\!\}]\,\mathrm{d}A = 0, \\
&\qquad\qquad \forall\delta\Theta\in\mathscr{H}^1(\mathcal{B}_0) \quad \text{and} \quad \forall\delta\overline{\Theta}\in\mathscr{H}^1(\mathcal{I}_0),
\end{aligned} \tag{12}$$

where $\overline{\boldsymbol{Q}}_0 = -\bar{J}\,\overline{\boldsymbol{F}}^{-1}\cdot\bar{\boldsymbol{k}}_0\cdot\overline{\boldsymbol{F}}^{-\mathrm{t}}\cdot\overline{\operatorname{Grad}}\,\overline{\Theta}$ is the undamaged heat conduction along the interface.

It is of great importance to mention that the current model can be simplified into other interface models. By setting the damage variable to zero, the model in [Kaessmair et al. 2014] is retrieved, where a nondegrading thermally GI and mechanically coherent energetic interface is studied. A degrading HC interface model is obtained as in [Esmaeili et al. 2016a] by setting $[\![\Theta]\!] = 0$, and consequently $\{\!\{\Theta\}\!\} = \overline{\Theta}$,

	bulk		interface	
Lamé constant:	μ	80193.8 N/mm^2	$\bar{\mu}$	2×80193.8 N/mm
Lamé constant:	λ	110743.5 N/mm^2	$\bar{\lambda}$	2×110743.5 N/mm
compression modulus:	κ	164206.03 N/mm^2	$\bar{\kappa}$	2×190937.3 N/mm
specific heat capacity:	$c_{\boldsymbol{F}}$	3.588 N/[mm^{2}K]	$\bar{c}^0_{\boldsymbol{F}}$	3.588 N/[mmK]
heat conduction coeff.:	k	45 N/[sK]	$\bar{k}_0$	100×45 Nmm/[sK]
heat expansion coeff.:	α	10^{-5} 1/K	$\bar{\alpha}$	$[0-1.5] \times 10^{-5}$ 1/K
initial temperature:	Θ_0	298 K	$\bar{\Theta}_0$	298 K

	only interface			
	$\bar{F}_0$	0.005	$\bar{F}_{\mathrm{f}}$	0.1
thermal resistance	$\bar{r}^0_Q$	0.1 mm sK/N	$\bar{R}$	0.1 mm

Table 3. Material properties assumed in the numerical examples. Note that $\kappa = \lambda + 2/3\,\mu$ and $\bar{\kappa} = \bar{\lambda} + \bar{\mu}$.

which then results in the last integral in (12) to vanish. A degrading LC interface can be modeled as in [Esmaeili et al. 2016b] by removing the second term in the last integral, due to the fact that the jump of normal heat flux across interface vanishes (see relation $(10)_2$). The finite element implementation is given in Appendix A.

5. Numerical examples

In this section we study the computational aspects of thermally GI and mechanically coherent energetic interfaces subject to in-plane degradation and their effects on the overall response of the body. The in- and out-of-plane thermomechanical response of the interface is affected by the interface in-plane degradation. In particular, we focus on the influence of interface damage on the out-of-plane thermal properties of the interface, i.e., $\bar{s}_0$ and $\bar{r}^0_Q$. It is important to point out that the solution procedure is robust and shows the asymptotically quadratic rate of convergence associated with the Newton–Raphson scheme. The computational domain is discretized using 1600 trilinear hexahedral elements.

The reversible material behavior in the bulk and on the interface is characterized by a thermohyperelastic Helmholtz energy functions. The damage affects the interface response by reducing the interface stiffness, heat capacity and heat conduction coefficient, and increasing the Kapitza coefficient $\bar{r}^0_Q$ and thermal sensitivity $\bar{s}_0$. Appendix B gathers the effective (undamaged) Helmholtz energy functions together with their corresponding derivatives both in the bulk and on the interface. The corresponding material parameters for the bulk and interface are given in Table 3.

Consider now the strip shown in Figure 4, where a constant displacement is prescribed at the two opposite faces. The strip is partitioned into two homogeneous domains by an interface. The width and the thickness of the strip are kept constant. The thermal boundary condition is globally adiabatic, i.e., $\widehat{\boldsymbol{Q}}^{\mathrm{p}} = \widetilde{\boldsymbol{Q}}^{\mathrm{p}} = \mathbb{0}$. The thermal initial condition is a uniformly distributed temperature $\Theta_0 = 298$ K. In order to better understand the influence of a thermomechanical GI interface on the overall response of the body, all thermomechanical properties of the bulk are fixed. Similar examples of intact (nondegrading)

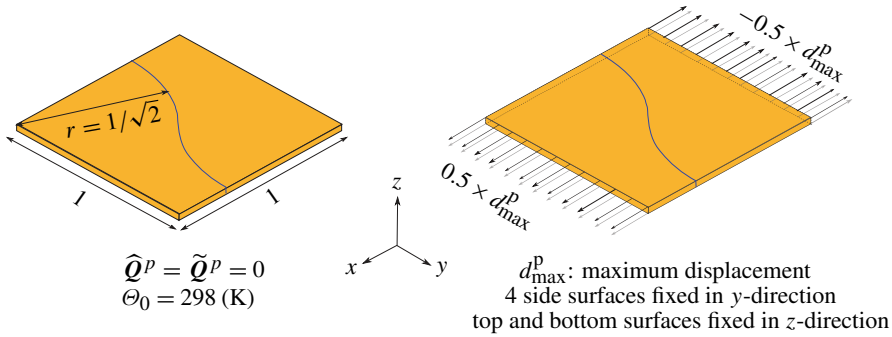

Figure 4. Strip with curved interface: geometry, left, and applied boundary conditions, right. Dimensions are in mm. The thickness is 0.05.

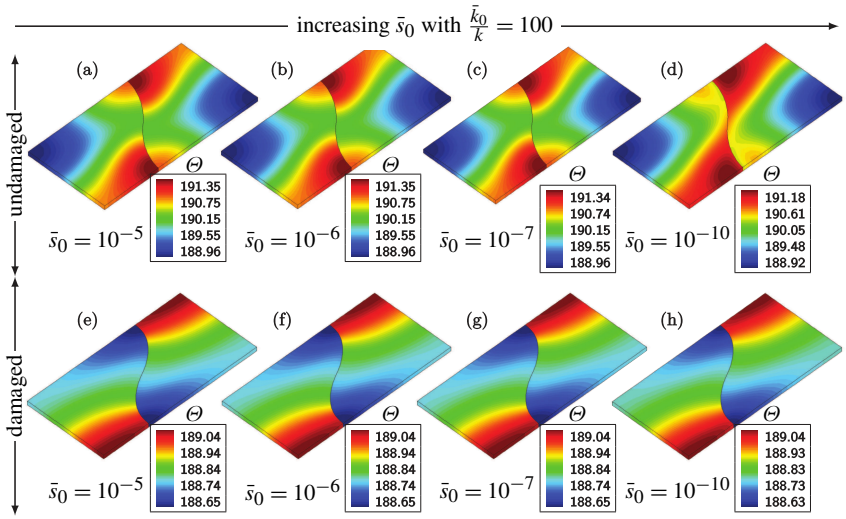

Figure 5. The bulk temperature distribution of the strip stretched up to 100% of its original length for $\bar{\mu}/\mu = \bar{\lambda}/\lambda = 2$ mm, $\bar{r}^0_Q = 0.1$ and $\bar{k}_0/k = 100$ mm. Results a–d correspond to the intact interface, whereas results e–h correspond to the degrading interface.

LC, HC and GI interfaces can be found respectively in [Javili et al. 2012; 2013; Kaessmair et al. 2014]. Degrading HC and LC interfaces are studied in the recent contributions [Esmaeili et al. 2016a; 2016b], respectively. It is mentioned that to obtain an HC interface behavior from the current model, one can assign infinitesimal values to $\bar{s}_0$ and $\bar{r}^0_Q$, which causes both dissipation contributions in (9) to vanish. An LC interface is obtained by setting only $\bar{s}_0 \approx 0$, while $\bar{r}^0_Q$ is assigned a finite value. Note that we use Fourier-like relations (10) to fulfill the inequalities in (9).

In the first example we focus on the conductivity of a degrading interface. The domain is stretched up to 100% of its initial length in 40 equal steps where the total time is 10 ms. Note that for this example, $c^0_{\bar{F}} = \bar{\alpha} = 0$ and $\bar{k}_0/k = 100$ mm, $\bar{r}^0_Q = 0.1$, and $\bar{s}_0$ varies from 10^{-5} to 10^{-10}. The results of the two cases, undamaged and damaged interface, are compared and depicted in Figure 5. It is observed that the temperature distribution along the intact interface is more uniform (see Figure 5a–d) than the

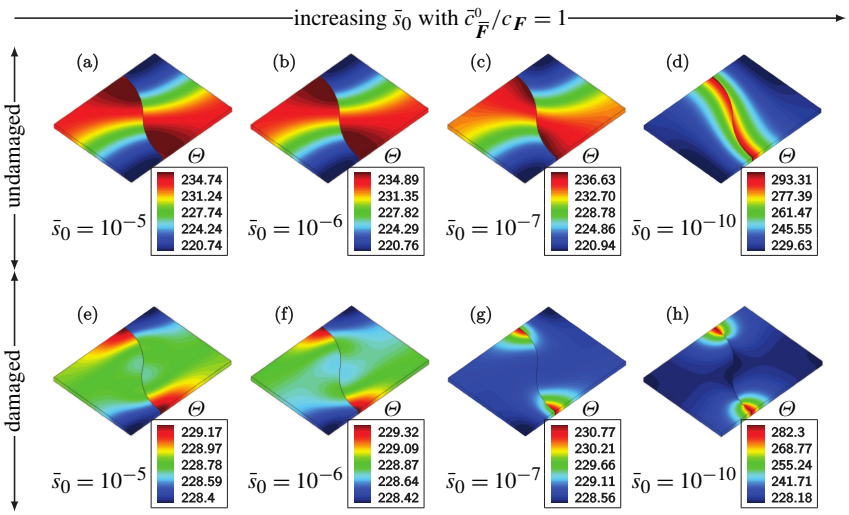

Figure 6. The bulk temperature distribution of the strip stretched up to 30% of its original length for $\bar{\mu}/\mu = \bar{\lambda}/\lambda = 2\,\text{mm}$, $\bar{r}^0_Q = 0.1$ and $c^0_{\bar{F}}/c_F = 1\,\text{mm}$. Results a–d correspond to the intact interface, whereas results e–h correspond to the degrading interface.

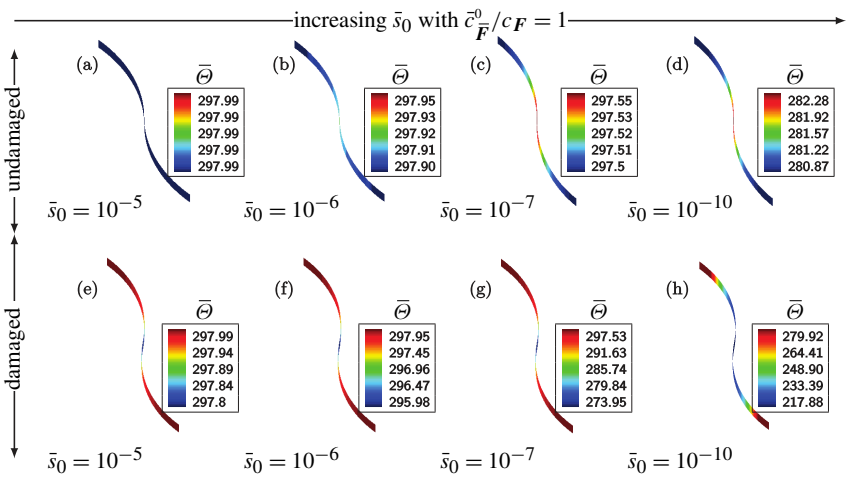

Figure 7. The interface temperature distribution of the strip stretched up to 30% of its original length for $\bar{\mu}/\mu = \bar{\lambda}/\lambda = 2$ mm, $\bar{r}^0_Q = 0.1$ and $c^0_{\bar{F}}/c_F = 1$ mm. Results a–d correspond to the intact interface, whereas results e–h correspond to the degrading interface.

one along the damaging interface (see Figure 5e–h). Moreover, a degrading interface causes a higher temperature jump across the interface due to the fact that $\bar{r}^0_Q/[1-\overline{D}_{\|}]$ assumes higher values as damage evolves. One should note that the simplified interface evolution equation of this example takes the form $\overline{\text{Div}}([1-\overline{D}_{\|}]\,\overline{\boldsymbol{Q}}) = -[\![\Theta]\!]$, thus a jump in the normal heat flux shall be observed. We point out that since the interface here is fully dissipative, in contrast to an HC interface, it allows for a jump in the

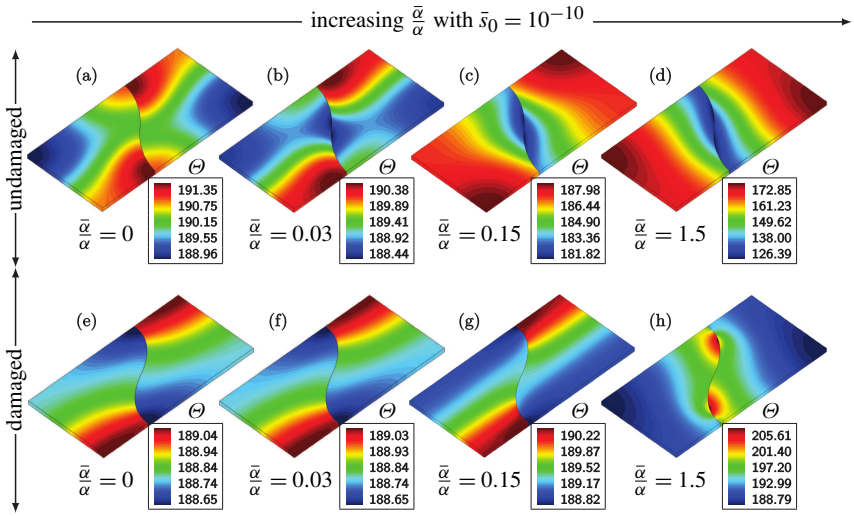

Figure 8. The bulk temperature distribution of the strip stretched up to 100% of its original length for $\bar{\mu}/\mu = \bar{\lambda}/\lambda = 2$ mm, $\bar{r}_Q^0 = 0.1$ and $\bar{s}_0 = 10^{-10}$. Results a–d correspond to the intact interface, whereas results e–h correspond to the degrading interface.

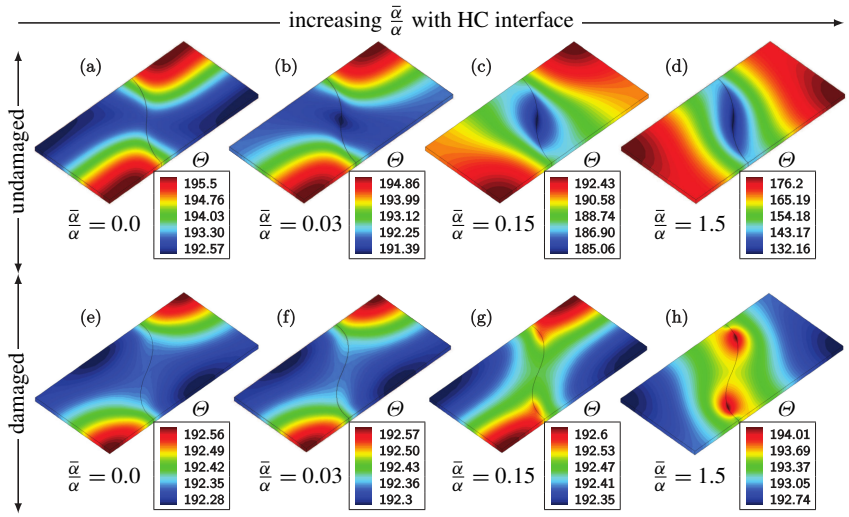

Figure 9. The bulk temperature distribution of the strip stretched up to 100% of its original length for $\bar{\mu}/\mu = \bar{\lambda}/\lambda = 2$ mm. Results a–d correspond to the intact highly conductive interface, whereas results e–h correspond to the degrading highly conductive interface. See [Esmaeili et al. 2016a] for further details.

temperature across the interface. Also, along a nondegrading HC interface with a high enough value for the interface conduction coefficient (such as $\bar{k}_0/k = 100$ mm), a uniform temperature distribution is achieved. This observation cannot be made for either an intact or a degrading GI interface (see Figure 5d and h, respectively).

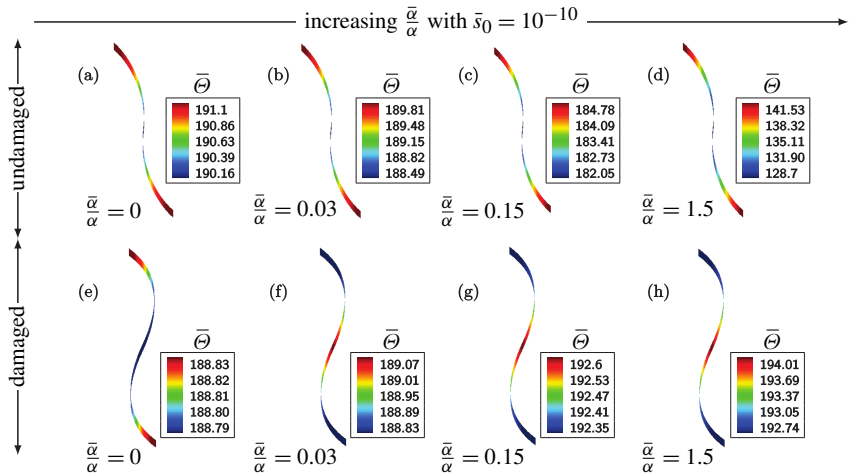

Figure 10. The interface temperature distribution of the strip stretched up to 100% of its original length for $\bar{\mu}/\mu = \bar{\lambda}/\lambda = 2$ mm, $\bar{r}^0_Q = 0.1$ and $\bar{s}_0 = 10^{-10}$. Results a–d correspond to the intact interface, whereas results e–h correspond to the degrading interface.

In the second example the effects of the interface heat capacity are studied. The domain here is stretched up to 30% of its initial length in 15 equal steps where the total time is 10 ms. Note that for this example, $\bar{k}_0 = \bar{\alpha} = 0$ and $\bar{c}^0_{\bar{\boldsymbol{F}}}/c_{\boldsymbol{F}} = 1$ mm, and $\bar{s}_0$ ranges from 10^{-5} to 10^{-10}. Analogous to the previous example, two cases of intact and damaged interface are considered here and shown in Figure 6 and Figure 7. From Figure 6 one finds that the intact interface is more capable of maintaining its initial temperature (also see Figure 7a–d). On the other hand, the domain cools down due to the Gough–Joule effect. These two different responses create the nonuniform temperature distribution in the domain containing the intact interface, as depicted in Figure 6a–d. On the contrary, a degrading interface can not retain its initial temperature (see Figure 7e–h), causing (in general) a more uniform temperature distribution in the domain as shown in Figure 6e–h. Note that for this example, the interface temperature evolution simplifies to $[1-\overline{D}_{\|}]\bar{c}^0_{\bar{\boldsymbol{F}}}\mathrm{D}_t\overline{\Theta} = -[\![\boldsymbol{Q}]\!]\cdot\bar{\boldsymbol{N}}$, meaning that a jump in the normal heat flux across the interface is present. Here we draw our attention to the difference between a thermally GI and HC interface. As mentioned before, an HC interface implies no temperature jump across the interface, and consequently the interface temperature becomes the average of the bulk temperatures on the two sides of the interface. Observing Figure 6 and Figure 7, one concludes that a jump in the temperature is clearly present across the interface, and the interface temperature is not the average of the surrounding bulk temperatures.

In the final example we turn our attention to the interface Gough–Joule effect by setting $\bar{k}_0 = \bar{c}^0_{\bar{\boldsymbol{F}}} = 0$ and $\bar{s}_0 = 10^{-10}$ and ranging $\bar{\alpha}/\alpha$ from 0 to 1.5. The domain here is stretched up to 100% of its initial length in 40 equal steps where the total time is 10 ms. The temperature evolution equation in this case simplifies to

$$[\![\boldsymbol{Q}]\!]\cdot\bar{\boldsymbol{N}} = \overline{\Theta}\partial_{\overline{\Theta}}([1-\overline{D}_{\|}]\bar{\boldsymbol{P}}_0) : \mathrm{D}_t\bar{\boldsymbol{F}} = \left[\overline{\Theta}[1-\overline{D}_{\|}]\partial_{\overline{\Theta}}P_0 - \overline{\Theta}\partial_{\overline{\Theta}}\overline{D}_{\|}\bar{\boldsymbol{P}}_0\right] : \mathrm{D}_t\bar{\boldsymbol{F}}.$$

From Figure 8 and Figure 10 we observe that the intact interface cools down under the increasing load due to the Gough–Joule effect more than the degrading interface. Moreover, it is shown that higher

temperature jumps and less strong coupling between the interface and bulk temperatures are achieved when the interface is allowed to degrade since

$$\bar{r}_Q^0/[1-\overline{D}_\parallel] \quad \text{and} \quad \bar{s}_0/[1-\overline{D}_\parallel]$$

assume higher values as damage evolves (compare Figure 8f–h to Figure 8a–d). Finally, the highest level of interface deformation is observed in this example due to the presence of the thermomechanical coupling term ($\bar{\alpha} \neq 0$) in the interface effective Helmholtz energy. A comparison is also made between a thermally GI and HC interface in Figure 9, which illustrates an HC interface under the same conditions as the thermally GI interface shown in Figure 8. The first observation, as expected, is the vanishing temperature jump across the HC interface. One can also notice that the HC interface (in general) retains to a larger extent its initial temperature. Although the intact thermally GI and HC interfaces have the lowest temperatures in the middle of the interface (see Figure 10a–d and Figure 9), the thermally GI interface temperature, unlike the HC interface temperature, is not coupled to its surrounding bulk temperatures. This means a thermally GI interface is allowed to be colder or warmer than the bulk (see Figure 10h and Figure 8h, where the interface is colder than the bulk). Note that for an HC interface the temperature is strongly coupled to that of the bulk by being the average of the adjacent bulk temperatures. Finally, the difference between a thermally GI and an HC interface becomes even more pronounced when in-plane degradation is allowed to initiate. Now, a degrading thermally GI interface loses its initial temperature at its two ends more drastically, while on an HC interface the coldest region is the middle of the interface.

6. Summary and conclusion

A theoretical and computational framework for continua containing thermally general imperfect and mechanically coherent energetic interfaces was outlined. The corresponding mechanical and thermal weak forms of the balance equations were given. The balance equations were fully discretized using the finite element method in space. The effects of the in-plane degradation on the in- and out-of-plane thermomechanical properties of the interface and the overall response of the body were also taken into account by introducing a tangential reduction factor. With the evolution of damage, the in-plane properties, i.e., interface stiffness, heat expansion coefficient, conduction coefficient and heat capacity coefficient, are reduced, whereas the out-of-plane properties, i.e., the Kapitza resistance coefficient and sensitivity, are increased. The increase of the out-of-plane thermal properties results in a higher temperature jump and a weaker coupling between interface and bulk temperatures. The tangential damage variable is a function of the equivalent distortion, which is nonlocalized using integral-type averaging.

A series of numerical examples served to elucidate the theory presented in this work. It was shown that the degraded interface undergoes more deformation. In addition, as the heat conduction coefficient is reduced while the damage evolves, higher temperature gradients along the interface were observed. It was also illustrated that an interface retains its initial temperature to a larger extent due to the reduced heat expansion coefficient. The degrading interface was shown to be less capable of being resistant to temperature changes as a result of the reduced specific heat capacity. We also observed that (in general) in all the examples higher temperature jumps across the interface and less strong coupling between the interface and bulk temperatures are attributed to the damage of the interface. Finally, in all the examples, asymptotically quadratic convergence associated with the Newton–Raphson scheme was achieved.

One consequent extension to this work is to study the role of the out-of-plane degradation of the interface material (cohesive damage) on the thermomechanical response of a thermally general imperfect and mechanically energetic interface. This includes introducing noncoherent deformation into the current formulation by allowing a displacement jump across the interface, which requires the use of a cohesive zone model. Such an extension shall be discussed in later contributions.

Appendix A: Finite element implementation

In order to apply the finite element method to the present problem, the weak forms (11) and (12) are discretized in space and time. The time interval $\mathcal{T}$ is subdivided into a set of intervals $\Delta t := t_{\tau+1} - t_\tau$ with

$$\mathcal{T} = \bigcup_{\tau=0}^{n_{\mathrm{ts}}} [t_\tau, t_{\tau+1}], \tag{A.1}$$

where n_{ts} denotes the number of time steps. The spatial discretization is performed using the Bubnov–Galerkin finite element method. The geometry and temperature of the bulk and interface together with the jump and average of temperature over the interface are approximated as a function of the natural coordinates $\xi \in [-1, 1]^3$ and $\bar{\xi} \in [-1, 1]^2$ assigned to the bulk and the interface, respectively. Using standard interpolations according to the isoparametric concepts, we obtain

$$\begin{aligned}
\boldsymbol{X}|_{\mathcal{B}_0^\beta} &\approx \boldsymbol{X}^{\mathrm{h}}(\xi) = \sum_{i=1}^{n_{\mathrm{nB}}} N^i(\xi)\boldsymbol{X}^i, & \overline{\boldsymbol{X}}|_{\mathcal{I}_0^\gamma} &\approx \overline{\boldsymbol{X}}^{\mathrm{h}}(\bar{\xi}) = \sum_{i=1}^{n_{\mathrm{nI}}} \overline{N}^i(\bar{\xi})\overline{\boldsymbol{X}}^i,\\
\boldsymbol{\varphi}|_{\mathcal{B}_0^\beta} &\approx \boldsymbol{\varphi}^{\mathrm{h}}(\xi) = \sum_{i=1}^{n_{\mathrm{nB}}} N^i(\xi)\boldsymbol{\varphi}^i, & \overline{\boldsymbol{\varphi}}|_{\mathcal{I}_0^\gamma} &\approx \overline{\boldsymbol{\varphi}}^{\mathrm{h}}(\bar{\xi}) = \sum_{i=1}^{n_{\mathrm{nI}}} \overline{N}^i(\bar{\xi})\overline{\boldsymbol{\varphi}}^i,\\
\Theta|_{\mathcal{B}_0^\beta} &\approx \Theta^{\mathrm{h}}(\xi) = \sum_{i=1}^{n_{\mathrm{nB}}} N^i(\xi)\Theta^i, & \overline{\Theta}|_{\mathcal{I}_0^\gamma} &\approx \overline{\Theta}^{\mathrm{h}}(\bar{\xi}) = \sum_{i=1}^{n_{\mathrm{nI}}} \overline{N}^i(\bar{\xi})\overline{\Theta}^i,\\
[\![\Theta]\!]|_{\mathcal{I}_0^\gamma} &\approx [\![\Theta]\!]^{\mathrm{h}}(\bar{\xi}) = \sum_{i=1}^{n_{\mathrm{nI}}} \overline{N}^i(\bar{\xi})[\![\Theta]\!]^i, & \{\!\{\Theta\}\!\}|_{\mathcal{I}_0^\gamma} &\approx \{\!\{\Theta\}\!\}^{\mathrm{h}}(\bar{\xi}) = \sum_{i=1}^{n_{\mathrm{nI}}} \overline{N}^i(\bar{\xi})\{\!\{\Theta\}\!\}^i,
\end{aligned} \tag{A.2}$$

where $\mathcal{B}_0^\beta$ and $\mathcal{I}_0^\gamma$ are the β^{th} and γ^{th} element in the bulk and on the interface, respectively. The shape functions of the bulk and interface elements at a local node i are denoted by N^i and $\overline{N}^i$, respectively. Every bulk and interface element consists of n_{nB} and n_{nI} nodes, respectively.

For the sake of brevity, homogeneous Neumann boundary conditions are assumed and hence some integrals vanish. The integrals are standard and require no additional care. Now, the fully discrete (spatially and temporally) form of mechanical and thermal residuals associated with the global node I are defined by

$$\begin{aligned}
[{}^{\mathrm{tot}}\boldsymbol{R}^I_{\boldsymbol{\varphi}}]_{\tau+1} = \int_{\mathcal{B}_0} \boldsymbol{P}_{\tau+1} \cdot \mathrm{Grad}\, N^I \,\mathrm{d}V - \int_{\mathcal{B}_0} N^I \boldsymbol{B}^{\mathrm{p}}_{\tau+1}\,\mathrm{d}V\\
+ \int_{\mathcal{I}_0} \left[[1 - \overline{D}_{\|}]\overline{\boldsymbol{P}}_0\right]_{\tau+1} \cdot \overline{\mathrm{Grad}}\, \overline{N}^I \,\mathrm{d}A - \int_{\mathcal{I}_0} \overline{N}^I \overline{\boldsymbol{B}}^{\mathrm{p}}_{\tau+1}\,\mathrm{d}A,
\end{aligned} \tag{A.3}$$

and

$$
\begin{aligned}
[{}^{\mathrm{tot}}\mathrm{R}^{I}_{\Theta}]_{\tau+1} = &-\int_{\mathcal{B}_0} \boldsymbol{Q}_{\tau+1}\cdot\mathrm{Grad}\,N^I + Q^{\mathrm{p}}_{\tau+1}N^I\,\mathrm{d}V - \int_{\mathcal{I}_0}\big[[1-D_{\|}]\,\overline{\boldsymbol{Q}}_0\big]_{\tau+1}\cdot\overline{\mathrm{Grad}}\,\overline{N}^I + \overline{Q}^{\mathrm{p}}_{\tau+1}\overline{N}^I\,\mathrm{d}A\\
&-\int_{\mathcal{B}_0}\Theta_{\tau+1}[\partial_{\Theta}\boldsymbol{P}]_{\tau+1} : \frac{1}{\Delta t}[\boldsymbol{F}_{\tau+1}-\boldsymbol{F}_{\tau}]N^I - c_{\boldsymbol{F}}\frac{1}{\Delta t}[\Theta_{\tau+1}-\Theta_{\tau}]N^I\,\mathrm{d}V\\
&-\int_{\mathcal{I}_0}\overline{\Theta}_{\tau+1}[\partial_{\overline{\Theta}}([1-\overline{D}_{\|}]\overline{\boldsymbol{P}}_0)]_{\tau+1} : \frac{1}{\Delta t}[\overline{\boldsymbol{F}}_{\tau+1}-\overline{\boldsymbol{F}}_{\tau}]\overline{N}^I - [1-\overline{D}_{\|}]\bar{c}^0_{\overline{\boldsymbol{F}}}\frac{1}{\Delta t}[\overline{\Theta}_{\tau+1}-\overline{\Theta}_{\tau}]\overline{N}^I\,\mathrm{d}A\\
&-\int_{\mathcal{I}_0}[1-\overline{D}_{\|}]\frac{1}{\bar{s}_0}[\overline{\Theta}^{-1}-\{\!\{\Theta^{-1}\}\!\}]\overline{N}^I\,\mathrm{d}A\\
&-\int_{\mathcal{I}^-_0}[1-\overline{D}_{\|}]\frac{1}{\bar{r}^0_Q}\overline{N}^I[\![\Theta]\!]_{\tau+1}\,\mathrm{d}A + \int_{\mathcal{I}^+_0}[1-\overline{D}_{\|}]\frac{1}{\bar{r}^0_Q}\overline{N}^I[\![\Theta]\!]_{\tau+1}\,\mathrm{d}A.
\end{aligned}
\tag{A.4}
$$

Note that mechanical and thermal residuals are composed of contributions from both the bulk and interface. Moreover, although the integrands of the last two integrals in (A.4) are identical, the domains over which these integrals are taken are different. This is due to the fact that the interface is thermally general imperfect. The global mechanical and thermal residual vectors take the form

$$
\begin{aligned}
&{}^{\mathrm{tot}}\boldsymbol{R} = [{}^{\mathrm{tot}}\boldsymbol{R}_{\boldsymbol{\varphi}}\ \boldsymbol{R}_{\Theta}\ {}^{\mathrm{tot}}\overline{\boldsymbol{R}}_{\overline{\Theta}}]^T \quad \text{with } {}^{\mathrm{tot}}\boldsymbol{R}_{\boldsymbol{\varphi}} = [\boldsymbol{R}^1_{\boldsymbol{\varphi}}\cdots\boldsymbol{R}^I_{\boldsymbol{\varphi}}\cdots\boldsymbol{R}^{n_{\mathrm{Bn}}}_{\boldsymbol{\varphi}}]^T + [\overline{\boldsymbol{R}}^1_{\boldsymbol{\varphi}}\cdots\overline{\boldsymbol{R}}^I_{\boldsymbol{\varphi}}\cdots\overline{\boldsymbol{R}}^{n_{\mathrm{In}}}_{\boldsymbol{\varphi}}]^T,\\
&\boldsymbol{R}_{\Theta} = [\mathrm{R}^1_{\Theta}\cdots\mathrm{R}^I_{\Theta}\cdots\mathrm{R}^{n_{\mathrm{Bn}}}_{\Theta}]^T \text{and } {}^{\mathrm{tot}}\overline{\boldsymbol{R}}_{\overline{\Theta}} = \underbrace{[\overline{\mathrm{R}}^1_{\Theta}\cdots\overline{\mathrm{R}}^I_{\Theta}\cdots\overline{\mathrm{R}}^{n_{\mathrm{In}}}_{\Theta}]^T}_{\overline{\boldsymbol{R}}_{\Theta}} + \underbrace{[\overline{\mathrm{R}}^{1^{\pm}}_{\Theta}\cdots\overline{\mathrm{R}}^{I^{\pm}}_{\Theta}\cdots\overline{\mathrm{R}}^{n^{\pm}_{\mathrm{In}}}_{\Theta}]^T}_{\overline{\boldsymbol{R}}_{\Theta^{\pm}}},
\end{aligned}
\tag{A.5}
$$

where n_{Bn} and n_{In} denote the number of bulk and interface nodes. The summation operator implies the (conventional) residual assembly of the finite element method. Note that total interface thermal residual ${}^{\mathrm{tot}}\overline{\boldsymbol{R}}_{\overline{\Theta}}$ is composed of contributions from interface residuals corresponding to the degrees of freedom $\overline{\Theta}$ and $\Theta^{\pm}$, respectively denoted by $\overline{\boldsymbol{R}}_{\overline{\Theta}}$ and $\overline{\boldsymbol{R}}_{\Theta^{\pm}}$. Both of the above thermal residuals contribute to the total thermal residual, i.e., ${}^{\mathrm{tot}}\boldsymbol{R}_{\Theta} = \boldsymbol{R}_{\Theta} + {}^{\mathrm{tot}}\overline{\boldsymbol{R}}_{\overline{\Theta}}$.

The fully discrete coupled nonlinear system of governing equations can be stated as follows:

$$
{}^{\mathrm{tot}}\boldsymbol{R}({}^{\mathrm{tot}}\boldsymbol{d}) \overset{!}{=} \mathbb{0} \quad \text{with} \quad {}^{\mathrm{tot}}\boldsymbol{d} = [\boldsymbol{d}_{\boldsymbol{\varphi}}\ \boldsymbol{d}_{\Theta}\ \boldsymbol{d}_{\overline{\Theta}}]^T,
\tag{A.6}
$$

where ${}^{\mathrm{tot}}\boldsymbol{d}$ is the unknown global vector of spatial coordinates $\boldsymbol{d}_{\boldsymbol{\varphi}}$ and temperature $\boldsymbol{d}_{\Theta}$ and $\boldsymbol{d}_{\overline{\Theta}}$. To solve $(\mathrm{A.6})_1$, a Newton–Raphson scheme is utilized. Thus, the consistent linearization of the resulting system of equations yields the total (algorithmic) tangent stiffness matrix for every pair of global nodes I and J as

$$
{}^{\mathrm{tot}}\boldsymbol{K}^{IJ} := \frac{\partial\,{}^{\mathrm{tot}}\boldsymbol{R}^I}{\partial\,{}^{\mathrm{tot}}\boldsymbol{d}^J} \quad \text{where} \quad {}^{\mathrm{tot}}\boldsymbol{K}^{IJ} = \begin{bmatrix} \boldsymbol{K}^{IJ}_{\boldsymbol{\varphi}\boldsymbol{\varphi}} & \boldsymbol{K}^{IJ}_{\boldsymbol{\varphi}\Theta} & \mathbb{0} \\ \boldsymbol{K}^{IJ}_{\Theta\boldsymbol{\varphi}} & \mathrm{K}^{IJ}_{\Theta\Theta} & 0 \\ \mathbb{0} & 0 & 0 \end{bmatrix} + \underbrace{\begin{bmatrix} {}^{\mathrm{tot}}\overline{\boldsymbol{K}}^{IJ}_{\boldsymbol{\varphi}\boldsymbol{\varphi}} & {}^{\mathrm{tot}}\overline{\boldsymbol{K}}^{IJ}_{\boldsymbol{\varphi}\Theta} & {}^{\mathrm{tot}}\overline{\boldsymbol{K}}^{IJ}_{\boldsymbol{\varphi}\overline{\Theta}} \\ {}^{\mathrm{tot}}\overline{\boldsymbol{K}}^{IJ}_{\Theta\boldsymbol{\varphi}} & {}^{\mathrm{tot}}\overline{\mathrm{K}}^{IJ}_{\Theta\Theta} & {}^{\mathrm{tot}}\overline{\mathrm{K}}^{IJ}_{\Theta\overline{\Theta}} \\ {}^{\mathrm{tot}}\overline{\boldsymbol{K}}^{IJ}_{\overline{\Theta}\boldsymbol{\varphi}} & {}^{\mathrm{tot}}\overline{\mathrm{K}}^{IJ}_{\overline{\Theta}\Theta} & {}^{\mathrm{tot}}\overline{\mathrm{K}}^{IJ}_{\overline{\Theta}\overline{\Theta}} \end{bmatrix}}_{{}^{\mathrm{tot}}\overline{\boldsymbol{K}}^{IJ}},
\tag{A.7}
$$

with ${}^{\mathrm{tot}}\overline{\boldsymbol{K}}^{IJ}$ being defined as

$$
\begin{bmatrix}
{}^{\mathrm{tot}}\overline{\boldsymbol{K}}^{IJ}_{\boldsymbol{\varphi}\boldsymbol{\varphi}} = \overline{\boldsymbol{K}}^{IJ}_{\boldsymbol{\varphi}\boldsymbol{\varphi}} & {}^{\mathrm{tot}}\overline{\boldsymbol{K}}^{IJ}_{\boldsymbol{\varphi}\Theta} = \overline{\boldsymbol{K}}^{IJ}_{\boldsymbol{\varphi}\Theta^+} + \overline{\boldsymbol{K}}^{IJ}_{\boldsymbol{\varphi}\Theta^-} & {}^{\mathrm{tot}}\overline{\boldsymbol{K}}^{IJ}_{\boldsymbol{\varphi}\overline{\Theta}} = \overline{\boldsymbol{K}}^{IJ}_{\boldsymbol{\varphi}\overline{\Theta}} \\
{}^{\mathrm{tot}}\overline{\boldsymbol{K}}^{IJ}_{\Theta\boldsymbol{\varphi}} = \overline{\boldsymbol{K}}^{IJ}_{\Theta^+\boldsymbol{\varphi}} + \overline{\boldsymbol{K}}^{IJ}_{\Theta^-\boldsymbol{\varphi}} & {}^{\mathrm{tot}}\overline{\mathrm{K}}^{IJ}_{\Theta\Theta} = \overline{\mathrm{K}}^{IJ}_{\Theta^+\Theta^+} + \overline{\mathrm{K}}^{IJ}_{\Theta^+\Theta^-} + \overline{\mathrm{K}}^{IJ}_{\Theta^-\Theta^+} + \overline{\mathrm{K}}^{IJ}_{\Theta^-\Theta^-} & {}^{\mathrm{tot}}\overline{\mathrm{K}}^{IJ}_{\Theta\overline{\Theta}} = \overline{\mathrm{K}}^{IJ}_{\Theta^+\overline{\Theta}} + \overline{\mathrm{K}}^{IJ}_{\Theta^-\overline{\Theta}} \\
{}^{\mathrm{tot}}\overline{\boldsymbol{K}}^{IJ}_{\overline{\Theta}\boldsymbol{\varphi}} = \overline{\boldsymbol{K}}^{IJ}_{\overline{\Theta}\boldsymbol{\varphi}} & {}^{\mathrm{tot}}\overline{\mathrm{K}}^{IJ}_{\overline{\Theta}\Theta} = \overline{\mathrm{K}}^{IJ}_{\overline{\Theta}\Theta^+} + \overline{\mathrm{K}}^{IJ}_{\overline{\Theta}\Theta^-} & {}^{\mathrm{tot}}\overline{\mathrm{K}}^{IJ}_{\overline{\Theta}\overline{\Theta}} = \overline{\mathrm{K}}^{IJ}_{\overline{\Theta}\overline{\Theta}}
\end{bmatrix}.
\tag{A.8}
$$

Note that ${}^{\mathrm{tot}}\boldsymbol{K}$ is also decomposed into contributions from the bulk and the interface. The bulk contributions to the total stiffness matrix are given as

$$
\begin{aligned}
\boldsymbol{K}^{IJ}_{\boldsymbol{\varphi}\boldsymbol{\varphi}} &= \frac{\partial \boldsymbol{R}^I_{\boldsymbol{\varphi}}}{\partial \boldsymbol{\varphi}^J} = \int_{\mathcal{B}_0} \operatorname{Grad} N^I \cdot\!\cdot [\partial_{\boldsymbol{F}} \boldsymbol{P}] \cdot \operatorname{Grad} N^J \,\mathrm{d}V, \quad \boldsymbol{K}^{IJ}_{\boldsymbol{\varphi}\Theta} = \frac{\partial \boldsymbol{R}^I_{\boldsymbol{\varphi}}}{\partial \Theta^J} = \int_{\mathcal{B}_0} N^J\, [\partial_{\Theta} \boldsymbol{P}] \cdot \operatorname{Grad} N^I \,\mathrm{d}V, \\
\boldsymbol{K}^{IJ}_{\Theta\boldsymbol{\varphi}} &= \frac{\partial \mathrm{R}^I_{\Theta}}{\partial \boldsymbol{\varphi}^J} = \int_{\mathcal{B}_0} -N^I \left[\frac{\partial (\Theta\, \partial_{\Theta} \boldsymbol{P} : \mathrm{D}_t \boldsymbol{F})}{\partial \boldsymbol{F}} \right] \cdot \operatorname{Grad} N^J - \operatorname{Grad} N^I \cdot [\partial_{\boldsymbol{F}} \boldsymbol{Q}] \cdot \operatorname{Grad} N^J \,\mathrm{d}V, \\
\mathrm{K}^{IJ}_{\Theta\Theta} &= \frac{\partial \mathrm{R}^I_{\Theta}}{\partial \Theta^J} = \int_{\mathcal{B}_0} -\operatorname{Grad} N^I \cdot \left[\frac{\partial \boldsymbol{Q}}{\partial \operatorname{Grad} \Theta} \right] \cdot \operatorname{Grad} N^J + N^I \left[\frac{c_{\boldsymbol{F}}}{\Delta t} - \left[\frac{\partial (\Theta\, \partial_{\Theta} \boldsymbol{P} : \mathrm{D}_t \boldsymbol{F})}{\partial \Theta} \right] \right] N^J \,\mathrm{d}V.
\end{aligned}
\tag{A.9}
$$

The interface contributions to the total stiffness matrix consist of local (${}^{\mathrm{loc}}\overline{\boldsymbol{K}}$) and nonlocal (${}^{\mathrm{nloc}}\overline{\boldsymbol{K}}$) contributions. The local contributions ${}^{\mathrm{loc}}\overline{\boldsymbol{K}}$, uniquely derived for a GI interface, are as follows:

$$
\begin{aligned}
{}^{\mathrm{loc}}\overline{\mathrm{K}}^{IJ}_{\Theta^{\pm}\overline{\Theta}} &= \frac{\partial \overline{\mathrm{R}}^{I^{\pm}}_{\Theta}}{\partial \overline{\Theta}^J} = \int_{\mathcal{I}_0^{\pm}} [1 - \overline{D}_{\parallel}(\bar{\boldsymbol{x}}_{\mathrm{r}})] \frac{1}{2\bar{s}_0} \frac{1}{\overline{\Theta}^2} \overline{N}^I \overline{N}^J \,\mathrm{d}A_{\mathrm{r}}, \\
{}^{\mathrm{loc}}\overline{\mathrm{K}}^{IJ}_{\overline{\Theta}\Theta^{\pm}} &= \frac{\partial \overline{\mathrm{R}}^I_{\overline{\Theta}}}{\partial \Theta^{J^{\pm}}} = \int_{\mathcal{I}_0} [1 - \overline{D}_{\parallel}(\bar{\boldsymbol{x}}_{\mathrm{r}})] \frac{1}{2\bar{s}_0} \frac{1}{[\Theta^{\pm}]^2} \overline{N}^I \overline{N}^J \,\mathrm{d}A_{\mathrm{r}}, \\
{}^{\mathrm{loc}}\overline{\mathrm{K}}^{IJ}_{\Theta^{\pm}\Theta^{\pm}} &= \frac{\partial \overline{\mathrm{R}}^{I^{\pm}}_{\Theta}}{\partial \Theta^{J^{\pm}}} = \int_{\mathcal{I}_0^{\pm}} [1 - \overline{D}_{\parallel}(\bar{\boldsymbol{x}}_{\mathrm{r}})] \frac{1}{4\bar{s}_0} \frac{1}{[\Theta^{\pm\pm}]^2} \overline{N}^I \overline{N}^J \,\mathrm{d}A_{\mathrm{r}} \pm \pm \int_{\mathcal{I}_0^{\pm}} [1 - \overline{D}_{\parallel}(\bar{\boldsymbol{x}}_{\mathrm{r}})] \frac{1}{\bar{r}^0_Q} \overline{N}^I \overline{N}^J \,\mathrm{d}A_{\mathrm{r}},
\end{aligned}
\tag{A.10}
$$

where $\mathrm{d}A_{\mathrm{r}} = \mathrm{d}A(\bar{\boldsymbol{x}}_{\mathrm{r}})$. The rest of interface local contributions to the total stiffness matrix are given as

$$
\begin{aligned}
{}^{\mathrm{loc}}\overline{\boldsymbol{K}}^{IJ}_{\boldsymbol{\varphi}\boldsymbol{\varphi}} &= \frac{\partial \overline{\boldsymbol{R}}^I_{\boldsymbol{\varphi}}}{\partial \overline{\boldsymbol{\varphi}}^J} = \int_{\mathcal{I}_0} \overline{\operatorname{Grad}}\, \overline{N}^I \cdot\!\cdot [1 - \overline{D}_{\parallel}(\bar{\boldsymbol{x}}_{\mathrm{r}})] \partial_{\overline{\boldsymbol{F}}} \overline{\boldsymbol{P}}_0(\bar{\boldsymbol{x}}_{\mathrm{r}}) \cdot \overline{\operatorname{Grad}}\, \overline{N}^J \,\mathrm{d}A_{\mathrm{r}}, \\
{}^{\mathrm{loc}}\overline{\boldsymbol{K}}^{IJ}_{\boldsymbol{\varphi}\overline{\Theta}} &= \frac{\partial \overline{\boldsymbol{R}}^I_{\boldsymbol{\varphi}}}{\partial \overline{\Theta}^J} = \int_{\mathcal{I}_0} \overline{N}^J [1 - \overline{D}_{\parallel}(\bar{\boldsymbol{x}}_{\mathrm{r}})] \partial_{\overline{\Theta}} \overline{\boldsymbol{P}}_0(\bar{\boldsymbol{x}}_{\mathrm{r}}) \cdot \overline{\operatorname{Grad}}\, \overline{N}^I \,\mathrm{d}A_{\mathrm{r}}, \\
{}^{\mathrm{loc}}\overline{\boldsymbol{K}}^{IJ}_{\overline{\Theta}\boldsymbol{\varphi}} &= \frac{\partial \overline{\mathrm{R}}^I_{\Theta}}{\partial \overline{\boldsymbol{\varphi}}^J} = \int_{\mathcal{I}_0} -\overline{N}^I [1 - \overline{D}_{\parallel}(\bar{\boldsymbol{x}}_{\mathrm{r}})] \left[\frac{\partial (\overline{\Theta}\, \partial_{\overline{\Theta}} \overline{\boldsymbol{P}}_0(\bar{\boldsymbol{x}}_{\mathrm{r}}) : \mathrm{D}_t \overline{\boldsymbol{F}})}{\partial \overline{\boldsymbol{F}}} \right] \cdot \overline{\operatorname{Grad}}\, \overline{N}^J \,\mathrm{d}A_{\mathrm{r}} \\
&\qquad - \int_{\mathcal{I}_0} \overline{N}^I [-\partial_{\overline{\Theta}} \overline{\mathcal{D}}_{\parallel}(\bar{\boldsymbol{x}}_{\mathrm{r}})] \left[\frac{\partial (\overline{\Theta}\, \overline{\boldsymbol{P}}_0(\bar{\boldsymbol{x}}_{\mathrm{r}}) : \mathrm{D}_t \overline{\boldsymbol{F}})}{\partial \overline{\boldsymbol{F}}} \right] \cdot \overline{\operatorname{Grad}}\, \overline{N}^J \mathrm{d}A_{\mathrm{r}} \\
&\qquad - \int_{\mathcal{I}_0} \overline{\operatorname{Grad}}\, \overline{N}^I \cdot [1 - \overline{D}_{\parallel}(\bar{\boldsymbol{x}}_{\mathrm{r}})] [\partial_{\overline{\boldsymbol{F}}} \overline{\boldsymbol{Q}}_0(\bar{\boldsymbol{x}}_{\mathrm{r}})] \cdot \overline{\operatorname{Grad}}\, \overline{N}^J \,\mathrm{d}A_{\mathrm{r}}, \\
{}^{\mathrm{loc}}\overline{\mathrm{K}}^{IJ}_{\overline{\Theta}\overline{\Theta}} &= \frac{\partial \overline{\mathrm{R}}^I_{\Theta}}{\partial \overline{\Theta}^J} = \int_{\mathcal{I}_0} -\overline{\operatorname{Grad}}\, \overline{N}^I \cdot [1 - \overline{D}_{\parallel}(\bar{\boldsymbol{x}}_{\mathrm{r}})] \left[\frac{\partial \overline{\boldsymbol{Q}}_0(\bar{\boldsymbol{x}}_{\mathrm{r}})}{\partial \overline{\operatorname{Grad}}\, \overline{\Theta}} \right] \cdot \overline{\operatorname{Grad}}\, \overline{N}^J \,\mathrm{d}A_{\mathrm{r}} \\
&\qquad + \int_{\mathcal{I}_0} \overline{N}^I [1 - \overline{D}_{\parallel}(\bar{\boldsymbol{x}}_{\mathrm{r}})] \left[\frac{\bar{c}^0_{\overline{\boldsymbol{F}}}}{\Delta t} + \frac{1}{\bar{s}_0 \overline{\Theta}^2} - \left[\frac{\partial (\overline{\Theta}\, \partial_{\overline{\Theta}} \overline{\boldsymbol{P}}_0(\bar{\boldsymbol{x}}_{\mathrm{r}}) : \mathrm{D}_t \overline{\boldsymbol{F}})}{\partial \overline{\Theta}} \right] \right] \overline{N}^J \,\mathrm{d}A_{\mathrm{r}} \\
&\qquad - \int_{\mathcal{I}_0} \overline{N}^I [-\partial_{\overline{\Theta}} \overline{\mathcal{D}}_{\parallel}(\bar{\boldsymbol{x}}_{\mathrm{r}})] \left[\frac{\partial (\overline{\Theta}\, \overline{\boldsymbol{P}}_0(\bar{\boldsymbol{x}}_{\mathrm{r}}) : \mathrm{D}_t \overline{\boldsymbol{F}})}{\partial \overline{\Theta}} \right] \overline{N}^J \,\mathrm{d}A_{\mathrm{r}},
\end{aligned}
\tag{A.11}
$$

where $\partial_{\bar{\Theta}}\bar{\mathcal{D}}_{\|}$, and using $(6)_{2,3}$, is computed as

$$\partial_{\bar{\Theta}}\bar{\mathcal{D}}_{\|}(\bar{\boldsymbol{x}}_{\mathrm{r}}) = \bar{\mathcal{D}}'_{\|}\partial_{\bar{\Theta}}F_{\mathrm{nloc}} \Rightarrow \partial_{\bar{\Theta}}F_{\mathrm{nloc}}(\bar{\boldsymbol{x}}_{\mathrm{r}}) = \int_{\mathcal{I}_0}\omega(\bar{\boldsymbol{x}}_{\mathrm{r}},\bar{\boldsymbol{x}}_{\mathrm{s}})\frac{1}{\bar{E}\,F_{\mathrm{loc}}(\bar{\boldsymbol{x}}_{\mathrm{s}})}\partial_{\bar{\Theta}}\bar{\Psi}^0(\bar{\boldsymbol{x}}_{\mathrm{s}})\,\mathrm{d}A_{\mathrm{s}} \tag{A.12}$$

with $\bar{\mathcal{D}}'_{\|} = \partial_{F_{\mathrm{nloc}}}\bar{\mathcal{D}}_{\|}$.

Next, the nonlocal corrections to the interface stiffness matrix are given as

$$\begin{aligned}
{}^{\mathrm{nloc}}\bar{\boldsymbol{K}}^{IJ}_{\boldsymbol{\varphi}\boldsymbol{\varphi}} &= \frac{\partial\bar{\boldsymbol{R}}^I_{\boldsymbol{\varphi}}}{\partial\bar{\boldsymbol{\varphi}}^J} = \int_{\mathcal{I}_0}\overline{\mathrm{Grad}}\,\bar{N}^I : \bar{\boldsymbol{P}}_0(\bar{\boldsymbol{x}}_{\mathrm{r}})\otimes[-\partial_{\bar{\boldsymbol{\varphi}}^J}\bar{\mathcal{D}}_{\|}(\bar{\boldsymbol{x}}_{\mathrm{r}})]\,\mathrm{d}A_{\mathrm{r}},\\
{}^{\mathrm{nloc}}\bar{\boldsymbol{K}}^{IJ}_{\boldsymbol{\varphi}\bar{\Theta}} &= \frac{\partial\bar{\boldsymbol{R}}^I_{\boldsymbol{\varphi}}}{\partial\bar{\Theta}^J} = \int_{\mathcal{I}_0}[-\partial_{\bar{\Theta}^J}\bar{\mathcal{D}}_{\|}(\bar{\boldsymbol{x}}_{\mathrm{r}})]\bar{\boldsymbol{P}}_0(\bar{\boldsymbol{x}}_{\mathrm{r}})\cdot\overline{\mathrm{Grad}}\,\bar{N}^I\,\mathrm{d}A_{\mathrm{r}},\\
{}^{\mathrm{nloc}}\bar{\boldsymbol{K}}^{IJ}_{\bar{\Theta}\boldsymbol{\varphi}} &= \frac{\partial\bar{\mathrm{R}}^I_{\Theta}}{\partial\bar{\boldsymbol{\varphi}}^J} = \int_{\mathcal{I}_0} -\bar{N}^I\bar{\Theta}\mathrm{D}_t\bar{\boldsymbol{F}} : [-\partial_{\bar{\Theta}}\bar{\boldsymbol{P}}_0\otimes\partial_{\bar{\boldsymbol{\varphi}}^J}\bar{\mathcal{D}}_{\|} - \bar{\boldsymbol{P}}_0\otimes\partial_{\bar{\boldsymbol{\varphi}}^J\bar{\Theta}}\bar{\mathcal{D}}_{\|}]_{\bar{\boldsymbol{x}}_{\mathrm{r}}}\,\mathrm{d}A_{\mathrm{r}}\\
&\qquad - \int_{\mathcal{I}_0}\overline{\mathrm{Grad}}\,\bar{N}^I\cdot\bar{\boldsymbol{Q}}_0(\bar{\boldsymbol{x}}_{\mathrm{r}})\otimes[-\partial_{\bar{\boldsymbol{\varphi}}^J}\bar{\mathcal{D}}_{\|}(\bar{\boldsymbol{x}}_{\mathrm{r}})]\\
&\qquad\quad + \bar{N}^I[-\partial_{\bar{\boldsymbol{\varphi}}^J}\bar{\mathcal{D}}_{\|}(\bar{\boldsymbol{x}}_{\mathrm{r}})]\left[\bar{c}^0_{\bar{\boldsymbol{F}}}\mathrm{D}_t\bar{\Theta} - \frac{1}{\bar{s}_0}[\bar{\Theta}^{-1} - \{\!\{\Theta\}\!\}^{-1}]\right]_{\bar{\boldsymbol{x}}_{\mathrm{r}}}\mathrm{d}A_{\mathrm{r}},\\
{}^{\mathrm{nloc}}\bar{\boldsymbol{K}}^{IJ}_{\Theta^{\pm}\boldsymbol{\varphi}} &= \frac{\partial\bar{\mathrm{R}}^{I^{\pm}}_{\Theta}}{\partial\bar{\boldsymbol{\varphi}}^J} = \int_{\mathcal{I}^{\pm}_0}\bar{N}^I[-\partial_{\bar{\boldsymbol{\varphi}}^J}\bar{\mathcal{D}}_{\|}(\bar{\boldsymbol{x}}_{\mathrm{r}})]\left[\frac{1}{2\bar{s}_0}[\bar{\Theta}^{-1} - \{\!\{\Theta\}\!\}^{-1}] \pm \frac{1}{\bar{r}^0_Q}[\![\Theta]\!]\right]_{\bar{\boldsymbol{x}}_{\mathrm{r}}}\mathrm{d}A_{\mathrm{r}},\\
{}^{\mathrm{nloc}}\bar{\mathrm{K}}^{IJ}_{\bar{\Theta}\bar{\Theta}} &= \frac{\partial\bar{\mathrm{R}}^I_{\Theta}}{\partial\bar{\Theta}^J} = \int_{\mathcal{I}_0} -\overline{\mathrm{Grad}}\,\bar{N}^I\cdot[-\partial_{\bar{\Theta}^J}\bar{\mathcal{D}}_{\|}(\bar{\boldsymbol{x}}_{\mathrm{r}})]\,\bar{\boldsymbol{Q}}_0(\bar{\boldsymbol{x}}_{\mathrm{r}})\\
&\qquad - \bar{N}^I\bar{\Theta}[-\partial_{\bar{\Theta}^J}\bar{\mathcal{D}}_{\|}\partial_{\bar{\Theta}}\bar{\boldsymbol{P}}_0 - \partial_{\bar{\Theta}^J\bar{\Theta}}\bar{\mathcal{D}}_{\|}\bar{\boldsymbol{P}}_0]_{\bar{\boldsymbol{x}}_{\mathrm{r}}} : \mathrm{D}_t\bar{\boldsymbol{F}}(\bar{\boldsymbol{x}}_{\mathrm{r}})\,\mathrm{d}A_{\mathrm{r}}\\
&\qquad\quad + \int_{\mathcal{I}_0}\bar{N}^I[-\partial_{\bar{\Theta}^J}\bar{\mathcal{D}}_{\|}(\bar{\boldsymbol{x}}_{\mathrm{r}})]\left[\bar{c}^0_{\bar{\boldsymbol{F}}}\mathrm{D}_t\bar{\Theta} - \frac{1}{\bar{s}_0}[\bar{\Theta}^{-1} - \{\!\{\Theta^{-1}\}\!\}]\right]_{\bar{\boldsymbol{x}}_{\mathrm{r}}}\mathrm{d}A_{\mathrm{r}},
\end{aligned} \tag{A.13}$$

where

$$\mathrm{D}_t\bar{\boldsymbol{F}} = \frac{[\bar{\boldsymbol{F}}_{\tau+1} - \bar{\boldsymbol{F}}_{\tau}]}{\Delta t} \quad\text{and}\quad \mathrm{D}_t\bar{\Theta} = \frac{[\bar{\Theta}_{\tau+1} - \bar{\Theta}_{\tau}]}{\Delta t}.$$

The notation $[\{\bullet\}]_{\bar{\boldsymbol{x}}_{\mathrm{r}}}$ means that the quantity $\{\bullet\}$ is evaluated at point $\bar{\boldsymbol{x}}_{\mathrm{r}}$. In the derivation of the nonlocal corrections to the interface stiffness matrix, the first and second derivatives of the damage variable with respect to the nodal coordinates and temperature $\bar{\boldsymbol{\varphi}}^J$ and $\bar{\Theta}^J$ at an arbitrary point $\bar{\boldsymbol{x}}_{\mathrm{r}}$ on the interface using $(6)_{2,3}$ are calculated as follows:

$$\partial_{\bar{\Theta}^J}\bar{\mathcal{D}}_{\|}(\bar{\boldsymbol{x}}_{\mathrm{r}}) = \bar{\mathcal{D}}'_{\|}\partial_{\bar{\Theta}^J}F_{\mathrm{nloc}} \Rightarrow \partial_{\bar{\Theta}^J}F_{\mathrm{nloc}}(\bar{\boldsymbol{x}}_{\mathrm{r}}) = \int_{\mathcal{I}_0}\omega(\bar{\boldsymbol{x}}_{\mathrm{r}},\bar{\boldsymbol{x}}_{\mathrm{s}})\frac{1}{\bar{E}\,F_{\mathrm{loc}}(\bar{\boldsymbol{x}}_{\mathrm{s}})}\partial_{\bar{\Theta}}\bar{\Psi}^0(\bar{\boldsymbol{x}}_{\mathrm{s}})\bar{N}^J(\bar{\boldsymbol{x}}_{\mathrm{s}})\,\mathrm{d}A_{\mathrm{s}}, \tag{A.14}$$

$$\partial_{\bar{\boldsymbol{\varphi}}^J}\bar{\mathcal{D}}_{\|}(\bar{\boldsymbol{x}}_{\mathrm{r}}) = \bar{\mathcal{D}}'_{\|}\partial_{\bar{\boldsymbol{\varphi}}^J}F_{\mathrm{nloc}} \Rightarrow \partial_{\bar{\boldsymbol{\varphi}}^J}F_{\mathrm{nloc}}(\bar{\boldsymbol{x}}_{\mathrm{r}}) = \int_{\mathcal{I}_0}\omega(\bar{\boldsymbol{x}}_{\mathrm{r}},\bar{\boldsymbol{x}}_{\mathrm{s}})\frac{1}{\bar{E}\,F_{\mathrm{loc}}(\bar{\boldsymbol{x}}_{\mathrm{s}})}\partial_{\bar{\boldsymbol{F}}}\bar{\Psi}^0(\bar{\boldsymbol{x}}_{\mathrm{s}})\cdot\overline{\mathrm{Grad}}\,\bar{N}^J(\bar{\boldsymbol{x}}_{\mathrm{s}})\,\mathrm{d}A_{\mathrm{s}}, \tag{A.15}$$

$$\begin{aligned}
\partial_{\bar{\boldsymbol{\varphi}}^J\bar{\Theta}}\bar{\mathcal{D}}_{\|}(\bar{\boldsymbol{x}}_{\mathrm{r}}) &= \bar{\mathcal{D}}''_{\|}\partial_{\bar{\Theta}}F_{\mathrm{nloc}}\partial_{\bar{\boldsymbol{\varphi}}^J}F_{\mathrm{nloc}} + \bar{\mathcal{D}}'_{\|}\partial_{\bar{\boldsymbol{\varphi}}^J\bar{\Theta}}F_{\mathrm{nloc}} \quad\text{and}\\
\partial_{\bar{\Theta}^J\bar{\Theta}}\bar{\mathcal{D}}_{\|}(\bar{\boldsymbol{x}}_{\mathrm{r}}) &= \bar{\mathcal{D}}''_{\|}\partial_{\bar{\Theta}^J}F_{\mathrm{nloc}}\partial_{\bar{\Theta}}F_{\mathrm{nloc}} + \bar{\mathcal{D}}'_{\|}\partial_{\bar{\Theta}^J\bar{\Theta}}F_{\mathrm{nloc}},
\end{aligned} \tag{A.16}$$

where $\overline{\mathscr{D}}''_{\|} = \partial_{F_{\mathrm{nloc}}} \overline{\mathscr{D}}'_{\|}$ and $\mathrm{d}A_{\mathrm{s}} = \mathrm{d}A(\bar{\boldsymbol{x}}_{\mathrm{s}})$ and

$$\partial_{\overline{\boldsymbol{\varphi}}^J \overline{\Theta}} F_{\mathrm{nloc}}(\bar{\boldsymbol{x}}_{\mathrm{r}}) = \int_{\mathcal{I}_0} \omega(\bar{\boldsymbol{x}}_{\mathrm{r}}, \bar{\boldsymbol{x}}_{\mathrm{s}}) \left[\frac{-1}{\overline{E}^2 F_{\mathrm{loc}}^3} \partial_{\overline{\boldsymbol{F}}} \overline{\Psi}^0 \partial_{\overline{\Theta}} \overline{\Psi}^0 + \frac{1}{\overline{E} F_{\mathrm{loc}}} \partial_{\overline{\boldsymbol{F}}\overline{\Theta}} \overline{\Psi}^0 \right]_{\bar{\boldsymbol{x}}_{\mathrm{s}}} \cdot \overline{\mathrm{Grad}}\, \overline{N}^J(\bar{\boldsymbol{x}}_{\mathrm{s}})\, \mathrm{d}A_{\mathrm{s}}, \tag{A.17}$$

$$\partial_{\overline{\Theta}^J \overline{\Theta}} F_{\mathrm{nloc}}(\bar{\boldsymbol{x}}_{\mathrm{r}}) = \int_{\mathcal{I}_0} \omega(\bar{\boldsymbol{x}}_{\mathrm{r}}, \bar{\boldsymbol{x}}_{\mathrm{s}}) \left[\frac{-1}{\overline{E}^2 F_{\mathrm{loc}}^3} [\partial_{\overline{\Theta}} \overline{\Psi}^0]^2 + \frac{1}{\overline{E} F_{\mathrm{loc}}} \partial_{\overline{\Theta}\overline{\Theta}} \overline{\Psi}^0 \right]_{\bar{\boldsymbol{x}}_{\mathrm{s}}} \overline{N}^J(\bar{\boldsymbol{x}}_{\mathrm{s}})\, \mathrm{d}A_{\mathrm{s}}. \tag{A.18}$$

Similarly the notation $[\{\bullet\}]_{\bar{\boldsymbol{x}}_{\mathrm{s}}}$ means that the quantity $\{\bullet\}$ is evaluated at point $\bar{\boldsymbol{x}}_{\mathrm{s}}$. Note that by using the derivatives (A.14)–(A.18) in the nonlocal corrections (A.13), the double integrals are introduced into the formulation due to nonlocality of the damage model. Furthermore, during unloading we set $\overline{\mathscr{D}}' = \overline{\mathscr{D}}'' = 0$.

Appendix B: Constitutive relations in the bulk and on the interface

bulk
$\Psi = \frac{1}{2}\lambda \ln^2 J + \frac{1}{2}\mu[\boldsymbol{F}:\boldsymbol{F} - 3 - 2\ln J] - 3\alpha\kappa[\Theta - \Theta_0]J^{-1}\ln J + c_{\boldsymbol{F}}[\Theta - \Theta_0 - \Theta\ln(\Theta/\Theta_0)] - \Xi_0[\Theta - \Theta_0]$
$\boldsymbol{P} = \lambda \ln J\, \boldsymbol{F}^{-\mathrm{t}} + \mu[\boldsymbol{F} - \boldsymbol{F}^{-\mathrm{t}}] - 3\alpha\kappa J^{-1}[\Theta - \Theta_0][1 - \ln J]\boldsymbol{F}^{-\mathrm{t}}$
$\Xi = 3\alpha\kappa J^{-1}\ln J + c_{\boldsymbol{F}} \ln(\Theta/\Theta_0) + \Xi_0$
$\partial_{\boldsymbol{F}} \boldsymbol{P} = \lambda[\boldsymbol{F}^{-\mathrm{t}} \otimes \boldsymbol{F}^{-\mathrm{t}} + \ln J\ \mathbb{D}] + \mu[\mathbb{I} - \mathbb{D}] + 3\alpha\kappa[\Theta - \Theta_0][J^{-1}[2 - \ln J]\boldsymbol{F}^{-\mathrm{t}} \otimes \boldsymbol{F}^{-\mathrm{t}} - J^{-1}[1 - \ln J]\mathbb{D}]$
$\partial_{\Theta} \boldsymbol{P} = -3\alpha\kappa J^{-1}[1 - \ln J]\boldsymbol{F}^{-\mathrm{t}}$
$\partial_{\Theta}(\Theta \partial_{\Theta} \boldsymbol{P} : \mathrm{D}_t \boldsymbol{F}) = -3\alpha\kappa J^{-1}[1 - \ln J]\,\mathrm{div}\, \boldsymbol{V}$
$\partial_{\boldsymbol{F}}(\Theta \partial_{\Theta} \boldsymbol{P} : \mathrm{D}_t \boldsymbol{F}) = -3\alpha\kappa\Theta[J^{-1}[\ln J - 2]\,\mathrm{div}\, \boldsymbol{V}\boldsymbol{F}^{-\mathrm{t}} + J^{-1}[1 - \ln J][\mathrm{D}_t \boldsymbol{F} : \mathbb{D} + [1/\Delta t]\boldsymbol{F}^{-\mathrm{t}} : \mathbb{I}]]$
$\partial_{\boldsymbol{F}} \boldsymbol{Q} = -Jk[\boldsymbol{F}^{-1} \cdot \boldsymbol{F}^{-\mathrm{t}} \otimes \boldsymbol{F}^{-\mathrm{t}} + \mathbb{B}] \underline{\cdot}\, \mathrm{Grad}\, \Theta,$ $\partial_{\mathrm{Grad}\,\Theta} \boldsymbol{Q} = -Jk\boldsymbol{G}$
$\mathbb{D} = \partial_{\boldsymbol{F}} \boldsymbol{F}^{-\mathrm{t}} = -\boldsymbol{F}^{-\mathrm{t}} \underline{\otimes}\, \boldsymbol{F}^{-1},$ $\mathbb{I} = \partial_{\boldsymbol{F}} \boldsymbol{F} = \boldsymbol{i} \overline{\otimes} \boldsymbol{I}$
$\mathbb{B} = \partial_{\boldsymbol{F}}(\boldsymbol{F}^{-1} \cdot \boldsymbol{F}^{-\mathrm{t}}) = -[\boldsymbol{F}^{-1} \overline{\otimes} \boldsymbol{F}^{-1}] \cdot \boldsymbol{F}^{-\mathrm{t}} - \boldsymbol{F}^{-1} \cdot [\boldsymbol{F}^{-\mathrm{t}} \underline{\otimes} \boldsymbol{F}^{-\mathrm{t}}],$ $\boldsymbol{G} = \boldsymbol{F}^{-1} \cdot \boldsymbol{F}^{-\mathrm{t}}$

interface
$\overline{\Psi}^0 = \frac{1}{2}\bar{\lambda}\ln^2 \bar{J} + \frac{1}{2}\bar{\mu}[\overline{\boldsymbol{F}}:\overline{\boldsymbol{F}} - 2 - 2\ln\bar{J}] - 2\bar{\alpha}\bar{\kappa}[\overline{\Theta} - \overline{\Theta}_0]\bar{J}^{-1}\ln\bar{J} + \bar{c}^0_{\overline{\boldsymbol{F}}}[\overline{\Theta} - \overline{\Theta}_0 - \overline{\Theta}\ln(\overline{\Theta}/\overline{\Theta}_0)] - \overline{\Xi}_{\mathrm{s}}[\overline{\Theta} - \overline{\Theta}_0]$
$\overline{\boldsymbol{P}}_0 = \partial_{\overline{\boldsymbol{F}}} \overline{\Psi}^0 = \bar{\lambda}\ln\bar{J}\,\overline{\boldsymbol{F}}^{-\mathrm{t}} + \bar{\mu}[\overline{\boldsymbol{F}} - \overline{\boldsymbol{F}}^{-\mathrm{t}}] - 2\bar{\alpha}\bar{\kappa}\bar{J}^{-1}[\overline{\Theta} - \overline{\Theta}_0][1 - \ln\bar{J}]\overline{\boldsymbol{F}}^{-\mathrm{t}}$
$\overline{\Xi}_0 = 2\bar{\alpha}\bar{\kappa}\bar{J}^{-1}\ln\bar{J} + \bar{c}^0_{\overline{\boldsymbol{F}}}\ln(\overline{\Theta}/\overline{\Theta}_0) + \overline{\Xi}_{\mathrm{s}},$ $\partial_{\overline{\Theta}} \overline{\Psi}^0 = -\overline{\Xi}_0$
$\partial_{\overline{\boldsymbol{F}}} \overline{\boldsymbol{P}}_0 = \bar{\lambda}[\overline{\boldsymbol{F}}^{-\mathrm{t}} \otimes \overline{\boldsymbol{F}}^{-\mathrm{t}} + \ln\bar{J}\,\overline{\mathbb{D}}] + \bar{\mu}[\overline{\mathbb{I}} - \overline{\mathbb{D}}] + 2\bar{\alpha}\bar{\kappa}[\overline{\Theta} - \overline{\Theta}_0][\bar{J}^{-1}[2 - \ln\bar{J}]\overline{\boldsymbol{F}}^{-\mathrm{t}} \otimes \overline{\boldsymbol{F}}^{-\mathrm{t}} - \bar{J}^{-1}[1 - \ln\bar{J}]\overline{\mathbb{D}}]$
$\partial_{\overline{\Theta}} \overline{\boldsymbol{P}}_0 = \partial_{\overline{\boldsymbol{F}}\overline{\Theta}} \overline{\Psi}^0 = -2\bar{\alpha}\bar{\kappa}\bar{J}^{-1}[1 - \ln\bar{J}]\overline{\boldsymbol{F}}^{-\mathrm{t}},$ $\partial_{\overline{\Theta}\overline{\Theta}} \overline{\Psi}^0 = -\bar{c}^0_{\overline{\boldsymbol{F}}} \overline{\Theta}^{-1}$
$\partial_{\overline{\Theta}}(\overline{\Theta} \partial_{\overline{\Theta}} \overline{\boldsymbol{P}}_0 : \mathrm{D}_t \overline{\boldsymbol{F}}) = -2\bar{\alpha}\bar{\kappa}\bar{J}^{-1}[1 - \ln\bar{J}]\,\overline{\mathrm{div}}\, \overline{\boldsymbol{V}}$
$\partial_{\overline{\boldsymbol{F}}}(\overline{\Theta} \partial_{\overline{\Theta}} \overline{\boldsymbol{P}}_0 : \mathrm{D}_t \overline{\boldsymbol{F}}) = -2\bar{\alpha}\bar{\kappa}\overline{\Theta}[\bar{J}^{-1}[\ln\bar{J} - 2]\,\overline{\mathrm{div}}\, \overline{\boldsymbol{V}}\,\overline{\boldsymbol{F}}^{-\mathrm{t}} + \bar{J}^{-1}[1 - \ln\bar{J}][\mathrm{D}_t \overline{\boldsymbol{F}} : \overline{\mathbb{D}} + [1/\Delta t]\overline{\boldsymbol{F}}^{-\mathrm{t}} : \bar{\mathbb{I}}]]$
$\partial_{\overline{\boldsymbol{F}}} \overline{\boldsymbol{Q}}_0 = -\bar{J}\bar{k}_0[\overline{\boldsymbol{F}}^{-1} \cdot \overline{\boldsymbol{F}}^{-\mathrm{t}} \otimes \overline{\boldsymbol{F}}^{-\mathrm{t}} + \overline{\mathbb{B}}] \underline{\cdot}\, \overline{\mathrm{Grad}}\, \overline{\Theta},$ $\partial_{\overline{\mathrm{Grad}}\,\overline{\Theta}} \overline{\boldsymbol{Q}}_0 = -\bar{J}\bar{k}_0 \overline{\boldsymbol{G}}$
$\overline{\mathbb{D}} = \partial_{\overline{\boldsymbol{F}}} \overline{\boldsymbol{F}}^{-\mathrm{t}} = -\overline{\boldsymbol{F}}^{-\mathrm{t}} \underline{\otimes}\, \overline{\boldsymbol{F}}^{-1} + [\boldsymbol{i} - \bar{\boldsymbol{i}}] \overline{\otimes}\, \overline{\boldsymbol{F}}^{-1} \cdot \overline{\boldsymbol{F}}^{-\mathrm{t}},$ $\bar{\mathbb{I}} = \partial_{\overline{\boldsymbol{F}}} \overline{\boldsymbol{F}} = \boldsymbol{i} \overline{\otimes} \bar{\boldsymbol{I}}$
$\overline{\mathbb{B}} = \partial_{\overline{\boldsymbol{F}}}(\overline{\boldsymbol{F}}^{-1} \cdot \overline{\boldsymbol{F}}^{-\mathrm{t}}) =^{\mathrm{t}} [\overline{\boldsymbol{F}}^{-1} \cdot \overline{\mathbb{D}}] + \overline{\boldsymbol{F}}^{-1} \cdot \overline{\mathbb{D}},$ $\overline{\boldsymbol{G}} = \overline{\boldsymbol{F}}^{-1} \cdot \overline{\boldsymbol{F}}^{-\mathrm{t}}$

List of symbols

$\boldsymbol{F}$	bulk material deformation gradient	$\overline{\boldsymbol{F}}$	interface material deformation gradient
$\boldsymbol{\varphi}$	bulk deformation map	$\overline{\boldsymbol{\varphi}}$	interface deformation map
$\boldsymbol{X}$	bulk material coordinates	$\overline{\boldsymbol{X}}$	interface material coordinates
$\boldsymbol{x}$	bulk spatial coordinates	$\overline{\boldsymbol{x}}$	interface spatial coordinates
Θ	bulk temperature	$\overline{\Theta}$	interface temperature
Θ_0	bulk initial temperature	$\overline{\Theta}_0$	interface initial temperature
$\boldsymbol{N}$	bulk material normal to surface	$\overline{\boldsymbol{N}}$	interface material normal to interface
$\boldsymbol{n}$	bulk spatial normal to surface	$\overline{\boldsymbol{n}}$	interface spatial normal to interface
Ψ	bulk Helmholtz energy	$\overline{\Psi}$	interface nominal Helmholtz energy
Ξ_{S}	bulk specific entropy	$\overline{\Xi}_{\mathrm{S}}$	interface specific entropy
Ξ	bulk entropy	$\overline{\Xi}$	interface nominal entropy
$\boldsymbol{P}$	bulk Piola stress	$\overline{\boldsymbol{P}}$	interface nominal Piola stress

only interface

$\boldsymbol{\varphi}^{\pm}$	deformation maps of $\pm$ side	$\boldsymbol{x}^{\pm}$	spatial coordinates of $\pm$ side
$\widetilde{\boldsymbol{n}}$	spatial normal to interface boundary	$\widetilde{\boldsymbol{N}}$	material normal to interface boundary
$\overline{\Psi}^0$	undamaged Helmholtz energy	$\overline{D}_{\parallel}$	damage variable
$\overline{\boldsymbol{P}}_0$	undamaged Piola stress tensor	$\overline{\Xi}^0$	undamaged entropy
$\overline{F}_{\mathrm{loc}}$	local equivalent distortion	$\overline{F}_{\mathrm{nloc}}$	nonlocal equivalent distortion
$\overline{F}_0$	elastic limit	$\overline{F}_{\mathrm{max}}$	maximum attained $\overline{F}_{\mathrm{nloc}}$
$\bar{s}_0$	undamaged sensitivity	$\bar{r}_Q^0$	undamaged Kapitza resistance coefficient

Acknowledgments

This research is performed as part of the Energie Campus Nuremberg and supported by funding through the "Bavaria on the Move" initiative of the state of Bavaria. The authors also gratefully acknowledge the support by the Cluster of Excellence "Engineering of Advanced Materials".

References

[Altenbach et al. 2012] H. Altenbach, V. A. Eremeyev, and N. F. Morozov, "Surface viscoelasticity and effective properties of thin-walled structures at the nanoscale", *Int. J. Eng. Sci.* **59** (2012), 83–89.

[Bažant and Jirásek 2002] Z. P. Bažant and M. Jirásek, "Nonlocal integral formulations of plasticity and damage: survey of progress", *J. Eng. Mech.* **128**:11 (2002), 1119–1149.

[Bažant and Xi 1991] Z. P. Bažant and Y. Xi, "Statistical size effect in quasi-brittle structures, II: Nonlocal theory", *J. Eng. Mech.* **117**:11 (1991), 2623–2640.

[Benveniste 2013] Y. Benveniste, "Models of thin interphases and the effective medium approximation in composite media with curvilinearly anisotropic coated inclusions", *Int. J. Eng. Sci.* **72** (2013), 140–154.

[Benveniste and Miloh 2001] Y. Benveniste and T. Miloh, "Imperfect soft and stiff interfaces in two-dimensional elasticity", *Mech. Mater.* **33**:6 (2001), 309–323.

[Berber et al. 2000] S. Berber, Y.-K. Kwon, and D. Tománek, "Unusually high thermal conductivity of carbon nanotubes", *Phys. Rev. Lett.* **84** (2000), 4613–4616.

[Cahill et al. 2003] D. G. Cahill, W. K. Ford, K. E. Goodson, G. D. Mahan, A. Majumdar, H. J. Maris, R. Merlin, and S. R. Phillpot, "Nanoscale thermal transport", *J. Appl. Phys.* **93** (2003), 793–818.

[Cammarata 1994] R. C. Cammarata, "Surface and interface stress effects in thin films", *Prog. Surf. Sci.* **46** (1994), 1–38.

[Chaboche 1981] J.-L. Chaboche, "Continuous damage mechanics — a tool to describe phenomena before crack initiation", *Nuc. Eng. Des.* **64**:2 (1981), 233–247.

[Che et al. 2000] J. Che, T. Çagin, and W. A. Goddard III, "Thermal conductivity of carbon nanotubes", *Nanotechnology* **11** (2000), 65–69.

[Daher and Maugin 1986] N. Daher and G. A. Maugin, "The method of virtual power in continuum mechanics: application to media presenting singular surfaces and interfaces", *Acta Mech.* **60**:3–4 (1986), 217–240.

[Davydov et al. 2013] D. Davydov, A. Javili, and P. Steinmann, "On molecular statics and surface-enhanced continuum modeling of nano-structures", *Comput. Mater. Sci.* **69** (2013), 510–519.

[dell'Isola and Romano 1987] F. dell'Isola and A. Romano, "On the derivation of thermomechanical balance equations for continuous systems with a nonmaterial interface", *Int. J. Eng. Sci.* **25**:11–12 (1987), 1459–1468.

[Dingreville et al. 2005] R. Dingreville, J. Qu, and M. Cherkaoui, "Surface free energy and its effect on the elastic behavior of nano-sized particles, wires and films", *J. Mech. Phys. Solids* **53**:8 (2005), 1827–1854.

[Duan et al. 2005a] H. L. Duan, J. Wang, Z. P. Huang, and B. L. Karihaloo, "Eshelby formalism for nano-inhomogeneities", *Proc. R. Soc. Lond. A* **461**:2062 (2005), 3335–3353.

[Duan et al. 2005b] H. L. Duan, J. Wang, Z. P. Huang, and B. L. Karihaloo, "Size-dependent effective elastic constants of solids containing nano-inhomogeneities with interface stress", *J. Mech. Phys. Solids* **53**:7 (2005), 1574–1596.

[Duan et al. 2009] H. L. Duan, J. Wang, and B. L. Karihaloo, "Theory of elasticity at the nanoscale", pp. 1–68 Elsevier, 2009.

[Esmaeili et al. 2016a] A. Esmaeili, A. Javili, and P. Steinmann, "Highly-conductive energetic coherent interfaces subject to in-plane degradation", *Math. Mech. Solids* (2016).

[Esmaeili et al. 2016b] A. Esmaeili, A. Javili, and P. Steinmann, "A thermo-mechanical cohesive zone model accounting for mechanically energetic Kapitza interfaces", *Int. J. Solids Struct.* **92–93** (2016), 29–44.

[Fischer and Svoboda 2010] F. D. Fischer and J. Svoboda, "Stresses in hollow nanoparticles", *Int. J. Solids Struct.* **47**:20 (2010), 2799–2805.

[Fried and Gurtin 2007] E. Fried and M. E. Gurtin, "Thermomechanics of the interface between a body and its environment", *Contin. Mech. Thermodyn.* **19**:5 (2007), 253–271.

[Fried and Todres 2005] E. Fried and R. E. Todres, "Mind the gap: the shape of the free surface of a rubber-like material in proximity to a rigid contactor", *J. Elasticity* **80**:1-3 (2005), 97–151.

[Gurtin 1998] M. E. Gurtin, "A general theory of curved deformable interfaces in solids at equilibrium", *Philos. Mag. A* **78**:5 (1998), 1093–1109.

[Gurtin and Murdoch 1975] M. E. Gurtin and A. I. Murdoch, "A continuum theory of elastic material surfaces", *Arch. Rational Mech. Anal.* **57**:4 (1975), 291–323.

[Huang and Sun 2007] Z. P. Huang and L. Sun, "Size-dependent effective properties of a heterogeneous material with interface energy effect: from finite deformation theory to infinitesimal strain analysis", *Acta Mech.* **190**:1–4 (2007), 151–163.

[Javili and Steinmann 2010] A. Javili and P. Steinmann, "On thermomechanical solids with boundary structures", *Int. J. Solids Struct.* **47**:24 (2010), 3245–3253.

[Javili et al. 2012] A. Javili, A. McBride, and P. Steinmann, "Numerical modelling of thermomechanical solids with mechanically energetic (generalised) Kapitza interfaces", *Comput. Mat. Sci.* **65** (2012), 542–551.

[Javili et al. 2013] A. Javili, A. McBride, and P. Steinmann, "Numerical modelling of thermomechanical solids with highly conductive energetic interfaces", *Int. J. Numer. Methods Eng.* **93**:5 (2013), 551–574.

[Javili et al. 2014] A. Javili, S. Kaessmair, and P. Steinmann, "General imperfect interfaces", *Comput. Methods Appl. Mech. Eng.* **275** (2014), 76–97.

[Kachanov 1958] L. M. Kachanov, "Time of the rupture process under creep conditions", *Izv. Akad. Nauk. S.S.R. Otd. Tech. Nauk.* **8** (1958), 26–31. In Russian; translated in *International Journal of Fracture* **97**:11 (1999), xi–xviii.

[Kaessmair et al. 2014] S. Kaessmair, A. Javili, and P. Steinmann, "Thermomechanics of solids with general imperfect coherent interfaces", *Arch. Appl. Mech.* **84**:9 (2014), 1409–1426.

[Levitas and Javanbakht 2010] V. I. Levitas and M. Javanbakht, "Surface tension and energy in multivariant martensitic transformations: phase-field theory, simulations, and model of coherent interface", *Phys. Rev. Lett.* **105**:16 (2010), 165701.

[Moeckel 1975] G. P. Moeckel, "Thermodynamics of an interface", *Arch. Rational Mech. Anal.* **57** (1975), 255–280.

[Murdoch 1976] A. I. Murdoch, "A thermodynamical theory of elastic material interfaces", *Quart. J. Mech. Appl. Math.* **29**:3 (1976), 245–275.

[Prasher 2005] R. Prasher, "Predicting the thermal resistance of nanosized constrictions", *Nano Letters* **5**:11 (2005), 2155–2159.

[Prasher 2006] R. Prasher, "Thermal interface materials: historical perspective, status, and future directions", *Proc. IEEE* **94**:8 (2006), 1571–1586.

[Rabotnov 1963] Y. N. Rabotnov, "On the equation of state of creep", *P. I. Mech. Eng. Conf. Proc.* **178**:1 (1963), 2–117–2–122.

[Sharma et al. 2003] P. Sharma, S. Ganti, and N. Bhate, "Effect of surfaces on the size-dependent elastic state of nano-inhomogeneities", *Appl. Phys. Lett.* **82**:4 (2003), 535–537.

[Simo and Hughes 1998] J. C. Simo and T. J. R. Hughes, *Computational inelasticity*, Springer, New York, 1998.

[de Souza Neto and Perić 1996] E. A. de Souza Neto and D. Perić, "A computational framework for a class of fully coupled models for elastoplastic damage at finite strains with reference to the linearization aspects", *Comput. Meth. Appl. Mech. Eng.* **130**:1 (1996), 179–193.

[de Souza Neto et al. 1998] E. A. de Souza Neto, D. Perić, and D. R. J. Owen, "Continuum modelling and numerical simulation of material damage at finite strains", *Arch. Comput. Methods Eng.* **5**:4 (1998), 311–384.

[Steigmann and Ogden 1999] D. J. Steigmann and R. W. Ogden, "Elastic surface-substrate interactions", *Proc. R. Soc. Lond. A* **455**:1982 (1999), 437–474.

[Steinmann 1999] P. Steinmann, "Formulation and computation of geometrically non-linear gradient damage", *Int. J. Num. Methods Eng.* **46**:5 (1999), 757–779.

[Steinmann 2008] P. Steinmann, "On boundary potential energies in deformational and configurational mechanics", *J. Mech. Phys. Solids* **56**:3 (2008), 772–800.

[Steinmann et al. 1994] P. Steinmann, C. Miehe, and E. Stein, "Comparison of different finite deformation inelastic damage models within multiplicative elastoplasticity for ductile materials", *Comput. Mech.* **13**:6 (1994), 458–474.

[Yvonnet et al. 2011] J. Yvonnet, A. Mitrushchenkov, G. Chambaud, and Q.-C. He, "Finite element model of ionic nanowires with size-dependent mechanical properties determined by ab initio calculations", *Comput. Methods Appl. Mech. Eng.* **200**:5–8 (2011), 614–625.

Received 23 Jun 2016. Revised 14 Nov 2016. Accepted 20 Nov 2016.

ALI ESMAEILI: ali.esmaeili@ltm.uni-erlangen.de
Department of Applied Mechanics, University of Erlangen-Nuremberg, Egerlandstrasse 5, D-91058 Erlangen, Germany

PAUL STEINMANN: paul.steinmann@ltm.uni-erlangen.de
Department of Applied Mechanics, University of Erlangen-Nuremberg, Egerlandstrasse 5, D-91058 Erlangen, Germany

ALI JAVILI: ajavili@bilkent.edu.tr
Department of Mechanical Engineering, Bilkent University, 06800 Ankara, Turkey

JOURNAL OF MECHANICS OF MATERIALS AND STRUCTURES

msp.org/jomms

Founded by Charles R. Steele and Marie-Louise Steele

See msp.org/jomms for submission guidelines.

JoMMS (ISSN 1559-3959) at Mathematical Sciences Publishers, 798 Evans Hall #6840, c/o University of California, Berkeley, CA 94720-3840, is published in 10 issues a year. The subscription price for 2017 is US $615/year for the electronic version, and $775/year (+$60, if shipping outside the US) for print and electronic. Subscriptions, requests for back issues, and changes of address should be sent to MSP.

JoMMS peer-review and production is managed by EditFLOW® from Mathematical Sciences Publishers.

PUBLISHED BY

mathematical sciences publishers

nonprofit scientific publishing

http://msp.org/

Journal of Mechanics of Materials and Structures
Volume 12, No. 3 May 2017